[redacted]

CCN

Technical Report No. 32-235

Studies of Chemical Propulsion Systems for Orbiting or Landing on the Moon and the Near Planets (U)

Allen D. Harper
Robert R. Breshears
Duane F. Dipprey
Joseph R. Wrobel

JET PROPULSION LABORATORY
CALIFORNIA INSTITUTE OF TECHNOLOGY
PASADENA, CALIFORNIA

March 15, 1962

[redacted]

CONFIDENTIAL

CONFIDENTIAL

[redacted]

NATIONAL AERONAUTICS AND SPACE ADMINISTRATION
CONTRACT NO. NAS 7-100

Technical Report No. 32-235

Studies of Chemical Propulsion Systems for Orbiting or Landing on the Moon and the Near Planets [redacted]

Allen D. Harper
Robert R. Breshears
Duane F. Dipprey
Joseph R. Wrobel

A. Briglio, Jr.

A. Briglio, *Chief*
Liquid Propulsion Section

JET PROPULSION LABORATORY
CALIFORNIA INSTITUTE OF TECHNOLOGY
PASADENA, CALIFORNIA

March 15, 1962

[redacted]

CONTENTS

TABLES

FIGURES

FIGURES (Cont'd)

FIGURES (Cont'd)

ABSTRACT

This report is a study of four spacecraft propulsion systems for use in conjunction with the currently proposed NASA vehicles, including the *Saturn* booster. Because of the implied time scale, no consideration is given to advanced systems utilizing nuclear systems for accelerating mass electrostatically, electromagnetically, or by direct heating. The systems considered represent the general classes of propulsion units suitable for spacecraft propulsion and are analyzed with emphasis on such aspects as over-all performance, configuration, operational reliability, and suitability for the space environment. A discussion is presented of the velocity requirements for orbiting and landing missions on the Moon and the near planets. The various systems are compared on the basis of payload performance capabilities for several selected missions.

I. INTRODUCTION

This publication is an outgrowth of a series of studies performed during 1961 by the Propulsion Systems Analysis Group of JPL's Liquid Propulsion Section. Although most of the subject studies have been generated to satisfy specific requirements, it is felt that a unification of these results into a more general treatment may be quite valuable. This document presents the results of such a compilation.

It is appropriate at this time to indicate the extent of these studies both in respect to the variety of missions considered and the types of systems examined. From the outset, one must realize that it is extremely difficult to make comparisons which remain valid over long periods because of such factors as unanticipated technological breakthroughs. For this reason the missions considered are limited to those which are scheduled to occur before 1966 in the Laboratory's plans for the next decade. This limits the range of spacecraft gross weights considered to those typical of *Centaur*- and *Saturn*-sized boost vehicles. Vehicles with smaller payload capability, such as the *Atlas-Agena*, are not considered, because their missions and designs are essentially frozen at this time. Larger vehicles (*Nova*) will not be operational until near or after the designated cutoff date, and their capabilities are not as yet clearly defined. Also it is believed that nuclear-powered boosters will not be available until after 1966.

Only chemical propulsion systems are discussed herein. It is believed that valuable conclusions may be reached under this ground rule only by eliminating from the list of missions to be analyzed the extremely-high-energy missions for which the electric propulsion systems should become competitive. Included in this category are the Mercury and Jupiter probes and the space probe out of the plane of the ecliptic. It is felt that the power supplies for the ion propulsion system may not have achieved the requisite state of development by 1966 to compete with chemical systems for the remaining missions.

Utilizing present concepts, spacecraft propulsion units may be classified into two subgroups. The first subclass may be called "correction devices," wherein the function is to make vernier-size corrections which nullify trajectory errors due to inaccuracies in the guidance system, propulsion system, or astronomical constants. The total velocity increment of these corrections is relatively small; therefore, the propulsion system mass will not be a large portion of the gross mass. This category of systems is not further discussed in this report; however, such a discussion may be found in Ref. 1.

The second subclassification may be called "retro propulsion devices." The function of these systems is to apply a braking velocity decrement to the spacecraft so that it will enter an orbit about the target body or will survive landing upon it. These devices characteristically require order-of-magnitude higher thrust levels than do the correction units. The subject matter of this report consists of descriptions and comparisons of propulsion systems which are suitable for the retro propulsion application.

In choosing the various chemical systems for comparison, an attempt has been made to select a representative member from each of the various classes of propellant combinations. From the class of storable propellants, the combination nitrogen tetroxide–hydrazine is chosen as representative of a group of relatively high-performance propellants which have received considerable development, *viz.*, combinations of oxidizers consisting of nitrogen oxides with hydrazine-based fuels. Systems containing pentaborane, which yield performance intermediate between the aforementioned storables and the fluorine–hydrazine system described below, are not considered, since it is believed that the state of development of this fuel is not sufficiently advanced at this time to enable a confident prediction of operational readiness by 1966.

The liquid oxygen–liquid hydrogen combination is chosen as representative of the class of extremely-low-temperature cryogenic propellants, since development effort on this combination is quite advanced, and its high potential performance has been experimentally obtained. Further, the performance is not so much lower than that of the fluorine–hydrogen system that the comparisons based on the O_2–H_2 system will be misleading, except for the very-high-energy missions which are not included in the present considerations.

The propellant combination fluorine–hydrazine, which exhibits a high combined density and a specific impulse intermediate between the storable and cryogenic liquids, is included to determine whether the characteristics of this system may combine to give desirable results.

To complete the spectrum of systems considered, a generalized solid-propellant motor is included in the comparisons. This is possible since the design factors for these motors are such that wide variations in parameters such as propellant composition, geometry, thrust, and burning time may be employed to satisfy a given framework of specifications. Therefore, it is possible to express the solid-propellant capabilities in the form of scaling coefficients and to make realistic predictions about future capabilities based upon past experience and present development trends.

Section II of this report discusses the operating requirements for these systems and indicates the extent to which these requirements are herein considered. A description of each of the various systems and scaling information for determination of system mass are presented in Section III. In Section IV, comparisons of the payload capabilities of the various systems are presented for several typical missions.

II. GENERAL SYSTEM CONSIDERATIONS

Presented here is a résumé of the requirements other than velocity increments which the spacecraft propulsion system must satisfy. The velocity increment requirements for the missions considered in this report are presented in an appendix.

Among the remaining requirements, meeting of launch schedules and reliability are paramount, especially in view of the infrequent opportunities for planetary missions and the limited number of launches anticipated. A few general conclusions on the philosophy of achieving reliability follow. First, since the reliability of a complex system is equal to the product of individual component reliabilities, simple systems such as either the solid system or the pressure-fed hypergolic liquid system will be favored. Second, if it is necessary to use a more complex system, it should probably be done in the boost phase rather than in the spacecraft propulsion phase. This is true because present plans call for multiple use of a relatively small number of different booster systems while the number of launchings of each spacecraft system will be small. Therefore, there will be considerably more opportunity to "debug" sophisticated systems when used in the booster systems than will be afforded in the spacecraft propulsion systems. One may also be certain that an unprecedented amount of testing will be required at all stages of development to assure that design specifications are satisfied. A single failure of any test will require, at the least, a comprehensive review of the design concept involved.

Among other considerations is the fact that on some missions multiple thrust chamber firings may prove advantageous. For most liquid systems, the requirement for repeated starts must be established at the outset. A single solid motor is presently not able to satisfy the restart requirement; however, this requirement may be avoided by the use of multiple motors. Another consideration is that the thrust buildup and tailoff transients must be short and pressure overshoots often cannot be tolerated. Further, the total impulse delivered during the shutdown transients must be highly reproducible, since this value must be built into the guidance system as a fixed bias.

Throttling over a range of thrust values may be a required characteristic on certain missions. At present there are no retro operations planned for which more than a limited amount of throttling—say to 80% of rated thrust—would be absolutely necessary. This may be easily accomplished with small loss of efficiency on most fixed-geometry liquid injectors by using a simple flow control valve in the propellant feed lines upstream of the injector. However, if an injector could be developed with a throttling range of 5:1, 20:1, or, even better, 100:1, it would allow a single propulsion system to fulfill several of the propulsion requirements of a given mission. It is believed that such a highly throttleable system would be a very desirable way of achieving over-all reliability through use of a simplified design. The development of an injector which could produce high performance at all flow settings would undoubtedly be classed as a breakthrough in injector design. It is almost certain that some method of varying injector orifice and/or thrust chamber nozzle areas will be required for this system. The solid systems cannot presently be throttled successfully.

A common requirement for all spacecraft propulsion systems is satisfactory ignition under zero g conditions. For systems employing liquid propellants, this requirement means that either some form of positive mechanical expulsion must be employed in the propellant feed system or that an additional system be added to create an acceleration field which would properly orient the propellants. The former system would be preferable from the reliability standpoint. The solid-propellant systems pose no problems in this respect.

A final requirement is that of satisfactory operation in the space environment. A prime consideration here is the hard vacuum, which may cause loss of material from surfaces due to evaporation, welding of adjacent metallic members, and greatly increased friction in mechanisms where there is relative motion between parts. It has not been established that high-energy cosmic radiation has deleterious effects on propellants and this may warrant study. Also, consideration must be given to the possibility of propulsion system damage from meteor collisions. Some form of temperature control system is needed to insure that liquid propellants will neither freeze nor produce excessive tank pressures, and that solid propellants will be maintained within a temperature range which will assure reproducible operation. A subproblem is the effect of strong ultraviolet radiation on paints commonly used as surface coatings to control radiative heat transfer.

III. SYSTEM DESCRIPTIONS

The characteristics of four propulsion systems are discussed in this section. Of these, three employ liquid propellants (nitrogen tetroxide–hydrazine, oxygen–hydrogen, and fluorine–hydrazine) and the fourth employs solid propellants. It may be noted that the approaches used in deriving the system designs differ slightly in various details. However, these differences are not substantial, and it is felt that the resulting comparisons are valid.

In deriving the mass estimates for these systems, a scaling equation of the following form has been assumed:

$$M_{ps} = \left(\frac{M_s}{M_p}\right) M_p + \left(\frac{M_f}{F}\right) F \qquad (1)$$

The scaling coefficients in Eq. (1) are presented in graphical form for each of the systems considered.

An indication of the relative sizes of the propulsion systems may be made by referring to the sketches which accompany the descriptions of the respective systems. The dimensions on these sketches were established by the propulsive requirements of a specific example retro mission (Ref. 2).

A. Nitrogen Tetroxide–Hydrazine System

The combination of nitrogen tetroxide (N_2O_4) as oxidizer and hydrazine (N_2H_4) as fuel is representative of the storable, hypergolic, liquid-propellant combinations which can provide simple and versatile spacecraft propulsion units. The basic system utilizes the N_2H_4 and N_2O_4 propellants stored within teflon bladders in aluminum propellant tanks. This system, designated the Advanced Liquid Propulsion System (ALPS) is presently under development at JPL. A single propellant tank version of this system is shown schematically in Fig. 1. The generant and its pressurizing gas are stored in a titanium pressure vessel with a butyl rubber bladder. During operation, the N_2H_4 is forced out of the generant tank by the expanding gas and is regulated to a constant gas-generator feed pressure. Heat is exchanged with the propellants to cool the gas-generator products to about 140°F before they are introduced into the propellant tank. The thrust chamber (with $L^* = 40$ in.) has been assumed to operate radiatively cooled. It is recognized that the use of such chambers will require a considerable development effort. The somewhat heavier alternative of an ablative design would probably be less of a development problem. Two chamber pressures (50 and 150 psia), three expansion ratios (20:1, 40:1, and 60:1), and two chamber materials (tungsten[1] and pyrolytic graphite) have been considered for mass and performance estimates. Table 1 lists specific impulse values assumed to be obtainable from various combinations of chamber pressure and expansion ratio. These values represent 94% of the theoretical equilibrium specific impulse.

Table 1. Specific impulse for nitrogen tetroxide–hydrazine system

Expansion ratio	Specific impulse, lbf-sec/lbm	
	Chamber pressure, 50 psia	Chamber pressure, 150 psia
20	309	305
40	321	317
60	328	323

The system mass estimates for this and the other liquid-propulsion systems were based upon the use of separate propellant tanks and their required structure. Recent unpublished studies have shown that the mass of a single integral propellant tank and its structure is about the same as that of the two separate propellant tanks and their supporting structure. The single and separate tank configurations are illustrated in Fig. 2. Both configurations shown are designed to meet the propulsive requirements of the example mission; the thrust chamber size was based on a chamber pressure of 150 psia, which was also employed for the system mass computations. No mass allowance has been made for thrust vector control or for interstage structure, which will vary somewhat with the different motor configurations. Size limitations of the spacecraft or shroud may determine the particular motor configuration to be used.

The coefficients (Eq. 1) for computing the propulsion system burnout mass for the N_2O_4–N_2H_4 system are given in Fig. 3–7. Figure 3 provides the propellant-scaled mass coefficient for chamber pressures of 150 and 50 psia. Figures 4 and 5 present the thrust-scaled mass coefficients for rocket chambers made of pyrolytic graphite with chamber pressures of 150 and 50 psia, respectively. Fig-

[1]The tungsten motor utilizes molybdenum and/or titanium wherever temperature and operation conditions permit (e.g., nozzle skirt extensions).

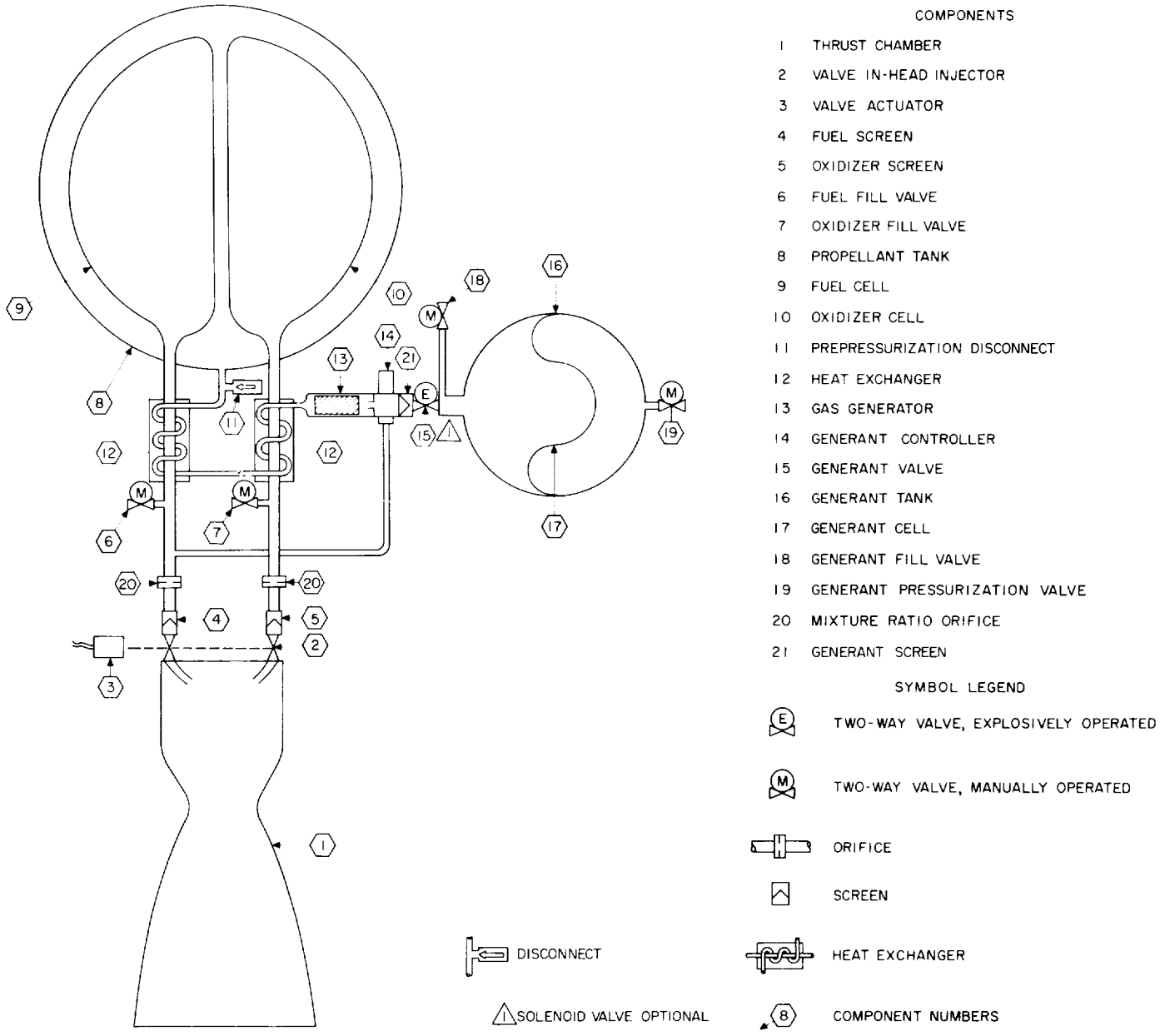

Fig. 1. Advanced liquid propulsion system schematic

ures 6 and 7 provide the same information for the use of tungsten chambers. It should be realized that the mass and performance figures discussed herein assume successful advanced developments in thrust chamber fabrication, propellant tankage, and tank bladders.

B. *Liquid Oxygen–Liquid Hydrogen System*

The characteristics of a system employing liquid hydrogen and liquid oxygen propellants are discussed in this section. A schematic diagram of this pumping system is presented in Fig. 8. The pressurization system is essentially the same as that conceived by Aerojet-General Corporation for use in the Hylas and Hylas-Star propulsion systems (Ref. 3, 4).[2] In this system, the oxidizer and auxiliary hydrogen are pumped by helium stored in a bottle inside the O_2 tank and warmed in a heat exchanger prior to entering the tank. The fuel is pumped by hydrogen stored in an auxiliary fuel tank inside the main fuel tank. This separate tank is used to sustain a pressure differential for pumping

[2]This is a proprietary development for which there is a patent pending.

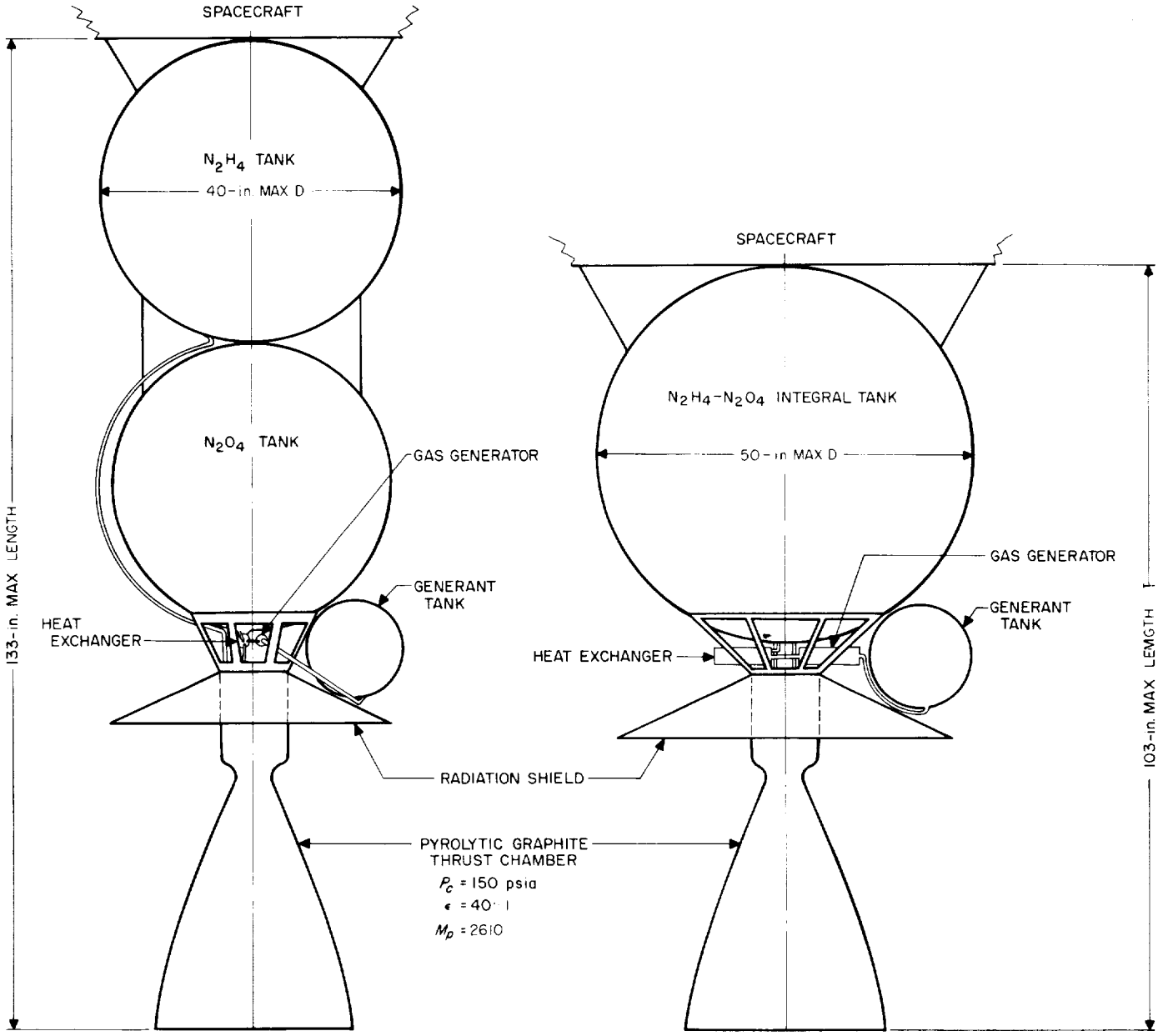

Fig. 2. Advanced liquid propulsion system (preliminary configuration)

the auxiliary fuel which is gasified in the heat exchanger. The propellants to run the gas generator, the products of which may serve as a heat source for the heat exchanger and as a means of roll control, are bled from the main propellant lines upstream of the thrust chamber.

The propellants are assumed to be housed in separate spherical tanks to eliminate the severe insulation problem encountered at a common bulkhead. This also permits optimization of the required insulation for each tank. At the outset, three materials were considered for tank fabrication: 2014-T6 aluminum with a yield stress of 80 ksi, stainless steel with a yield stress of 180 ksi, and titanium with a yield stress of 120 ksi. Because of the strength/density relationship, the relative masses of the tanks with reference to aluminum were 1.0, 1.36, and 0.96, respectively. On this basis, the titanium material looked slightly better than the aluminum. However, for many cases the resulting thickness of the tank wall was below that allowed by present fabrication techniques and ground handling operations with tanks in an unpressurized state. The value of minimum allowable effective

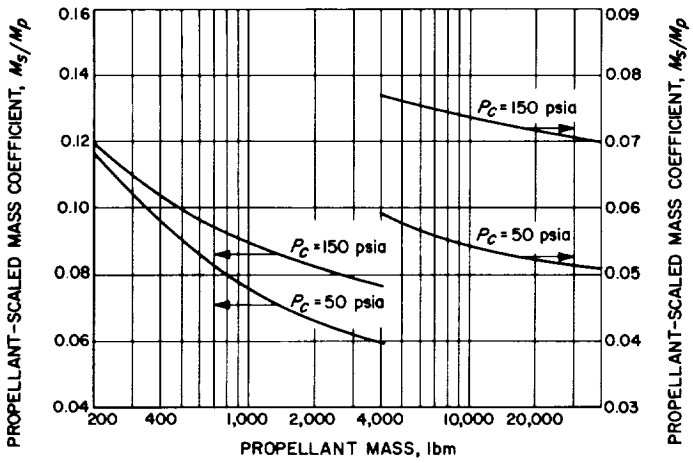

Fig. 3. Propellant-scaled mass coefficient as a function of propellant mass for a N_2O_4–N_2H_4 bipropellant rocket

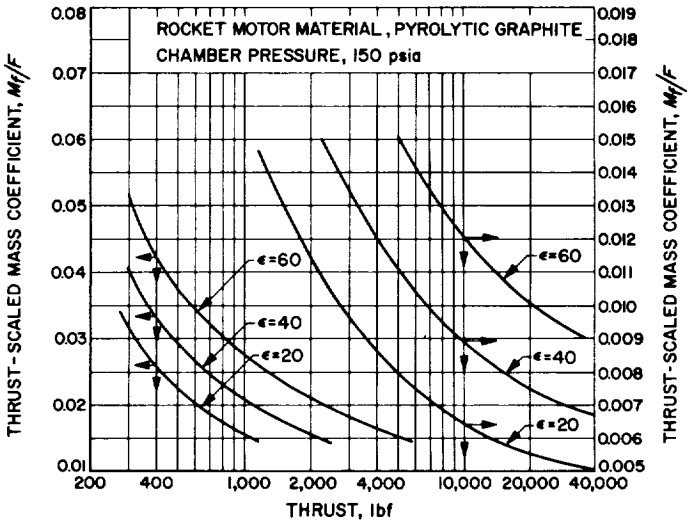

Fig. 4. Thrust-scaled mass coefficient as a function of thrust for a N_2O_4–N_2H_4 bipropellant rocket

thickness assumed for this study was 0.030 in. For a typical case of a thickness-limited tank, calculations of the relative masses yielded values of 1.0 for the aluminum, 1.45 for the titanium, and 2.58 for the stainless alloy. Therefore, the 2014-T6 aluminum material was selected since, at worst, it was only slightly heavier. The propellant-scaled mass coefficients for the oxygen–hydrogen system are based on this material.

Chamber pressures of 50 and 150 psia were considered for this system since these are expected to yield near minimum system mass. The thrust chamber was assumed to be fabricated from pyrolytic graphite. An engine expansion ratio of 40 was chosen as a practical compromise between increased performance and increased over-all system length. Under these conditions, it was assumed that a specific impulse of 430 sec—approximately 94% of the theoretical shifting equilibrium value—could be realized. Performances of this order have been experimentally obtained (Ref. 5).

Several mixture ratios from 3:1 to 7:1 were considered for a typical case, and their effect on over-all payload was determined. A mixture ratio of 5:1 was found to result in maximum payload capacity and reasonable tank size for the hydrogen. Therefore, this value of mixture ratio is used in the numerical examples presented herein.

In the determination of the geometrical arrangement of this stage, the predominant consideration was that of

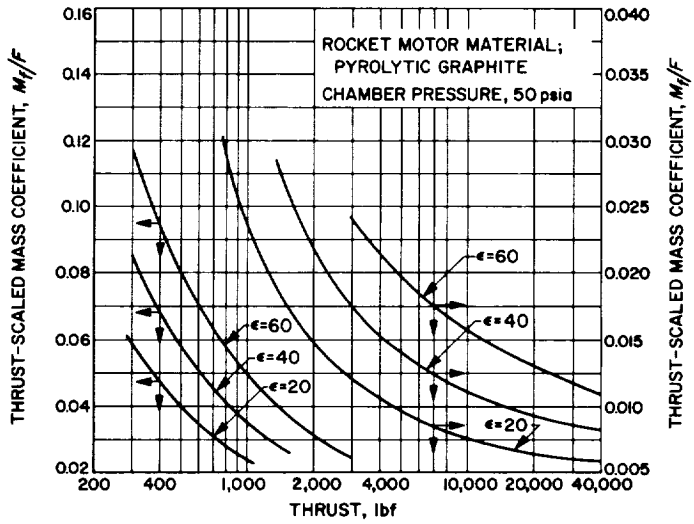

Fig. 5. Thrust-scaled mass coefficient as a function of thrust for a N_2O_4–N_2H_4 bipropellant rocket

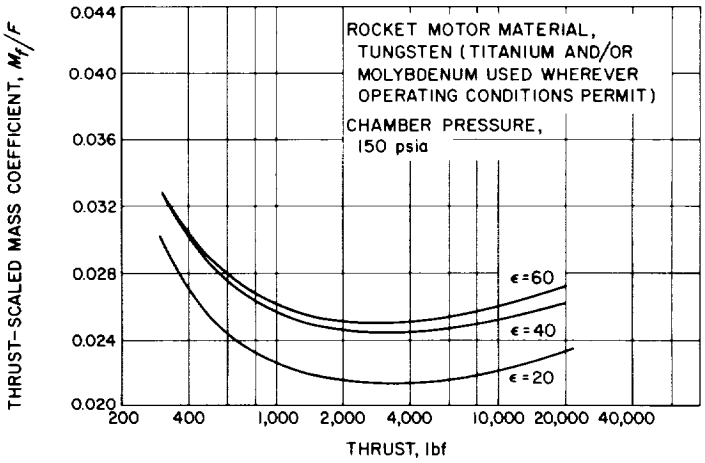

Fig. 6. Thrust-scaled mass coefficient as a function of thrust for a N_2O_4–N_2H_4 bipropellant rocket

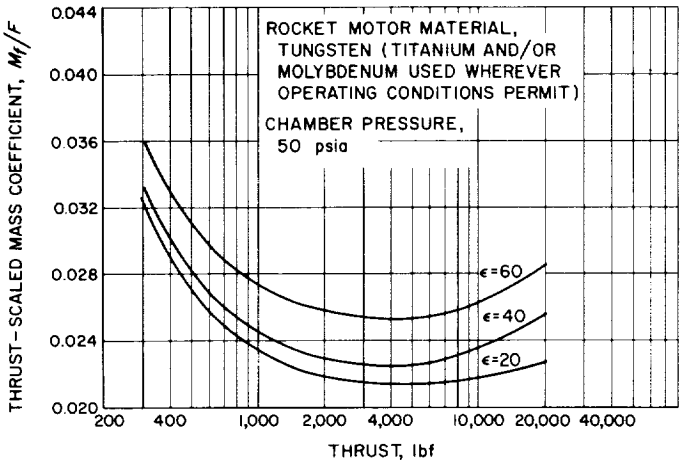

Fig. 7. Thrust-scaled mass coefficient as a function of thrust for a N_2O_4–N_2H_4 bipropellant rocket

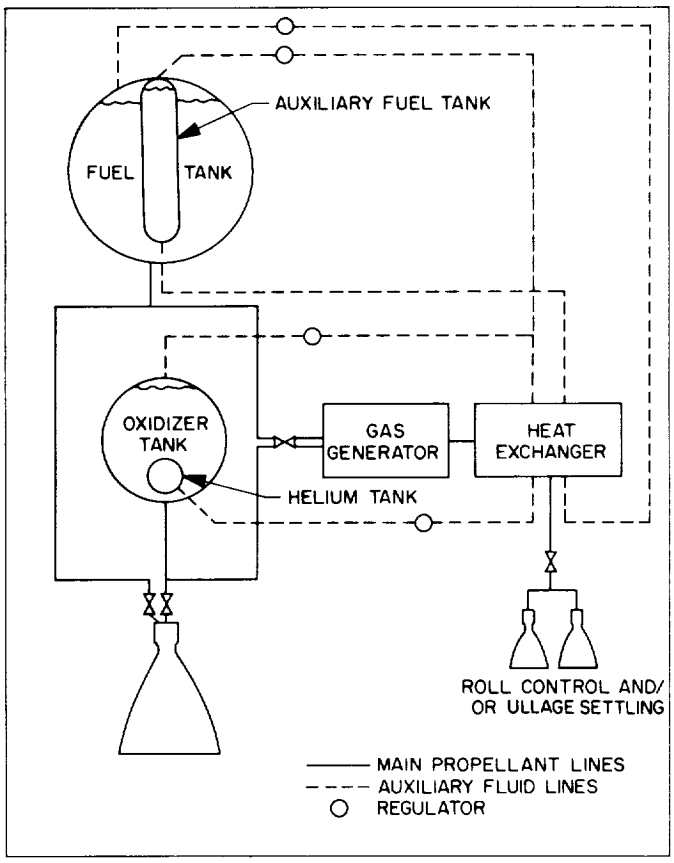

Fig. 8. Oxygen–hydrogen propulsion system schematic

heat transfer. Successful storage of the cryogenic propellants in space requires that the net heat gain of the propellants be minimized. The tank surface area must be minimized to reduce the incident solar heat load. Plumbing and structural attachments to the tanks must present minimum conduction paths from warm components of the spacecraft. Separate tanks are assumed in order to reduce the heat exchange deriving from the 200°F temperature differential between the propellants. Since the insulations proposed for these applications are nonrigid, the boost loads may not be transmitted through the insulation. Considerations such as these have dictated a stage geometry such as that illustrated in Fig. 9, where the chamber size is predicated upon a combustion chamber pressure of 50 psia and an expansion ratio of 40:1.

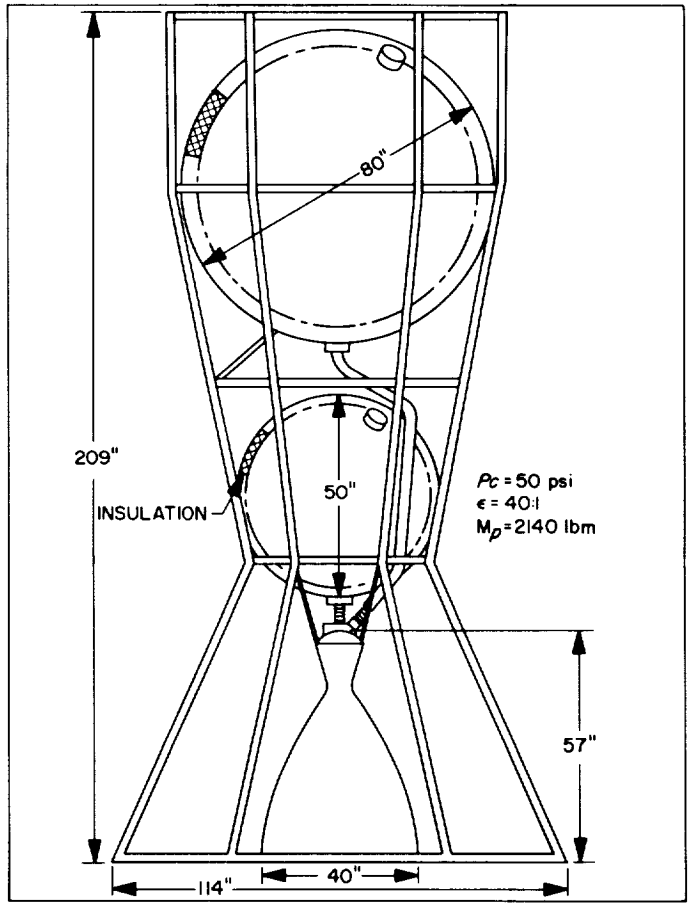

Fig. 9. Oxygen–hydrogen propulsion system (preliminary configuration)

The load-carrying structure of this stage is designed on the basis of existing state-of-the-art structural technology. The members are assumed to be fabricated of aluminum and to be capable of withstanding a longitudinal acceleration of 10 *g*. A simplified stress analysis of the members was conducted to estimate this contribution to the system mass. An allowance was made for the interstage structure and is included in the mass breakdown to provide a fair comparison with the other systems, since

the somewhat greater volume of this system would require more interstage structure. Fiberglass has been considered as an alternate structural material because of its low thermal conductivity. A fiberglass structure of comparable strength is of nearly the same mass as aluminum, although the members would be somewhat different in design. The effect of fiberglass exposure to a space environment has not been investigated thoroughly, and so it may not be recommended without some reservation. To reduce the conduction of heat into the propellant tank during storage, it is assumed that the tanks could be suspended within the spaceframe on four fiberglass rods and that the propellant lines leading into the tanks could be made of the same material, suitably coated if necessary to prevent interactions with the propellants. Possibly, the space environment problem could also be solved by surface coatings.

Prior to rocket ignition, it is recognized that a propellant settling maneuver will be necessary. Here, several methods are possible. One of the most convenient and efficient would be to start the small auxiliary gas generator prior to main engine firing and divert the hot gas products to properly oriented reaction nozzles. Another technique of possible interest would be to allow the fuel, used in chilling down the system hardware prior to ignition, to flow through the thrust chamber, thus providing a settling acceleration of about 0.02 g. A combination of both of the techniques described could be used with little additional complexity. On these bases, it is assumed that it would not be necessary to make additional mass allowances for the propellant settling manuever.

To store the cryogenic propellants, it is necessary to apply enough insulation to lower the net heat transfer rate into the propellant tanks enough so that the propellant vapor pressure does not exceed the operating pressure of the tanks. For this report, a layer of one of the several "super insulations"[3] was designed so that the propellants could be stored for the duration of the mission without venting the propellant tanks. The storage times implied for the Mars, Venus, and Moon missions were assumed to be 300, 150, and 3 days, respectively.

For the oxygen–hydrogen system, the propellant-scaled coefficient M_s/M_p is resolved into two parts, one due to the pumping and tankage system and one to the insulation, as follows:

$$M_s/M_p = M_{sf}/M_p + M_{if}/M_p \qquad (2)$$

[3]For example, Linde SI-4 or NCR-2.

The system-fraction coefficient M_{sf}/M_p is presented in Fig. 10 for systems with chamber pressures of 50 and 150 psia. The insulation-fraction coefficient M_{if}/M_p is presented in Fig. 11 and the thrust-scaled coefficient is presented in Fig. 12, both for the same chamber pressures. Chamber pressure appears as a parameter in Fig. 11 since, for the assumed pressurized system, the allowable propellant temperature rise is dependent upon the tank pressure, which in turn is determined by the chamber pressure. The propulsion system mass for the oxygen–hydrogen system may be calculated by inserting these coefficients into Eq. (1) and (2).

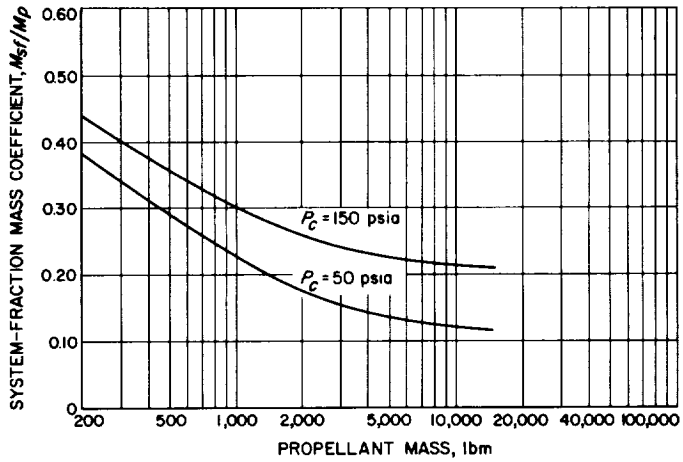

Fig. 10. System-fraction mass coefficient as a function of propellant mass for a pressure-fed oxygen–hydrogen propulsion system

C. *Fluorine–Hydrazine or Hydrazine Derivative System*

In this section a description is presented of the liquid system employing the propellant combination of fluorine as oxidizer and a hydrazine-based fuel. The use of such a propellant combination is presently under investigation at the Bell Aerosystems Laboratory. The fuel being considered is a blend of hydrazine, monomethyl hydrazine, and water. This blend is reputed to be superior to pure hydrazine with respect to thermal stability, heat transfer properties, and operating temperature range. The maximum vacuum specific impulse of this combination is approximately 4% less than that of pure hydrazine and fluorine. Maximum theoretical impulse occurs at an oxidizer/fuel mixture ratio of approximately 2.4. The mixture ratio selected for the present study, chosen on the basis of Bell's regenerative chamber cooling results, is 1.83. The attainable specific impulse, for calculation pur-

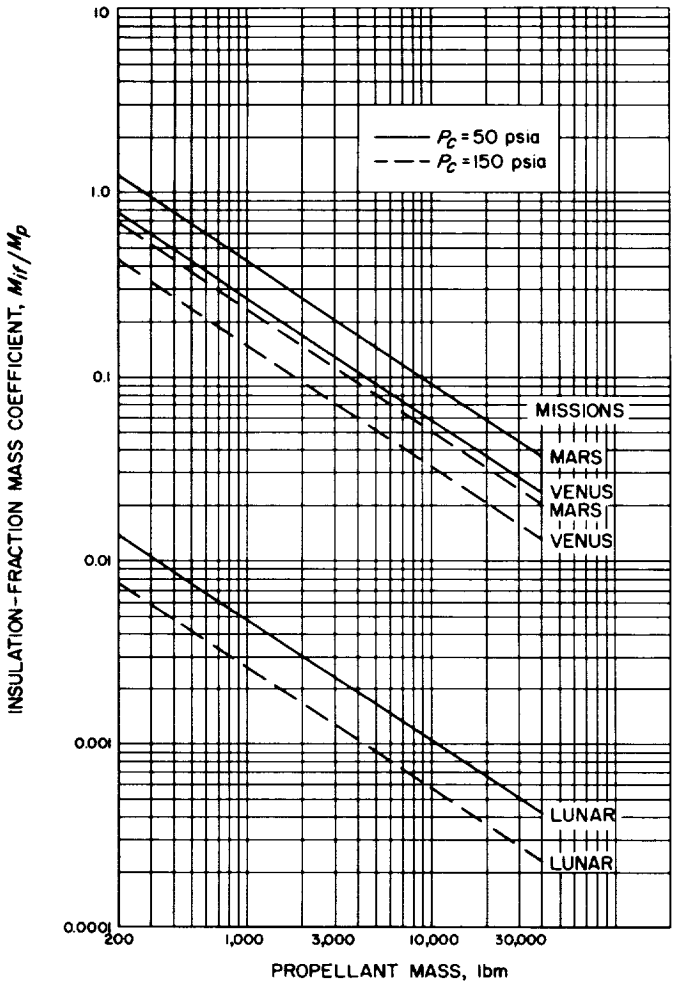

Fig. 11. Insulation-fraction mass coefficient for an oxygen–hydrogen propulsion system

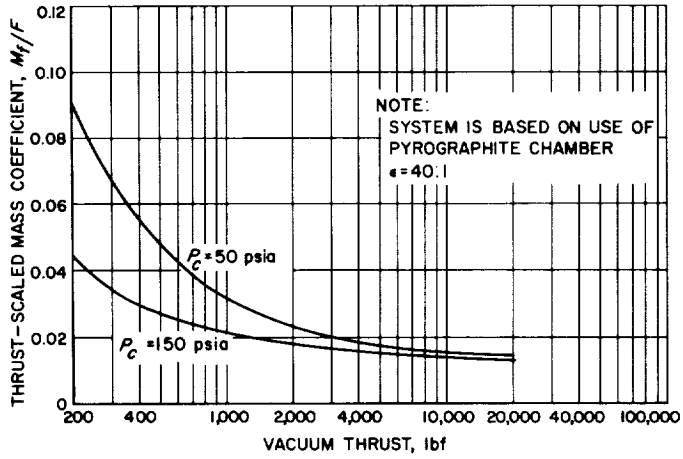

Fig. 12. Thrust-scaled mass coefficient for a pressure-fed oxygen–hydrogen propulsion system

poses, is 377 lbf-sec/lbm[4], which represents approximately 92% of maximum equilibrium impulse for this mixture ratio. Both Bell and the NASA-Lewis Laboratory have attained comparable combustion efficiencies with fluorine (Ref. 6).

The propellant supply system selected for this stage was chosen on the basis of simplicity of design and compatibility with the chemically reactive, cryogenic oxidizer. A simplified schematic of the propellant supply system is presented in Fig. 13. A similar supply system had been previously proposed for use with fluorine by Rocketdyne (Ref. 7). For the range of stage sizes considered, a gas-pressurized supply system was considered to be simpler and smaller than a pumped version. Helium was selected as the pumping medium because it is chemically inert and noncondensing. The helium is stored in

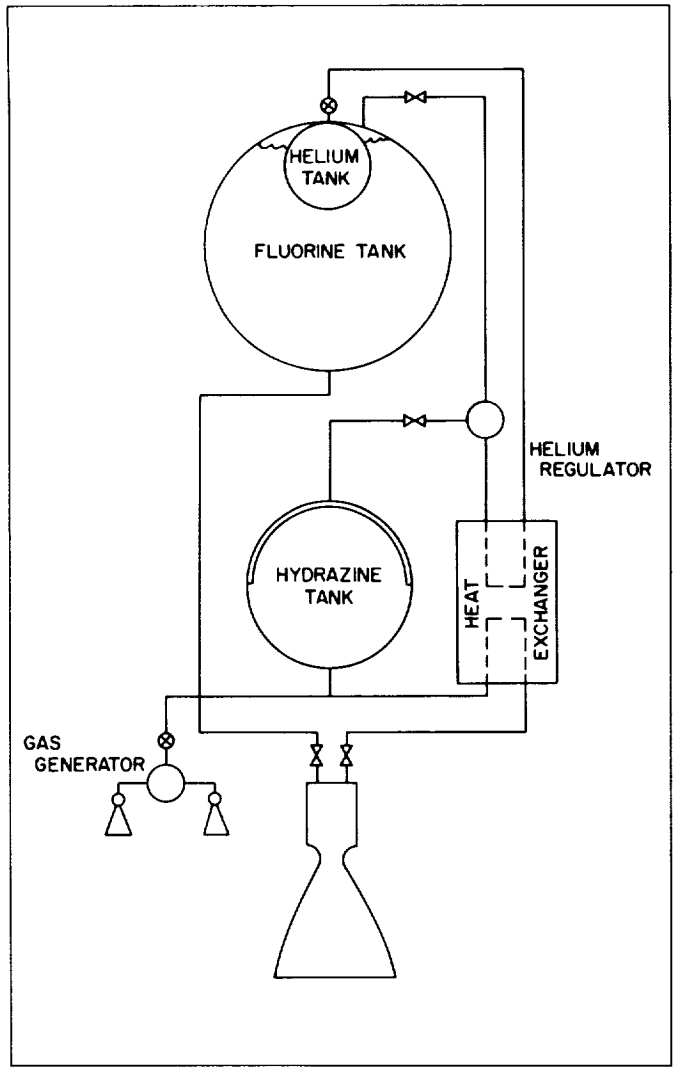

Fig. 13. Fluorine–hydrazine system schematic

[4]At 150-psia chamber pressure, 40:1 expansion to vacuum.

the oxidizer tank to take advantage of the higher density available at this low temperature. The gas, initially at 3000 psia, is passed through a heat exchanger incorporated in the hot fuel return lines of the regeneratively cooled engine and warmed to approximately 70°F prior to introduction into the propellant tanks. The use of heated helium minimizes the pumping gas requirement. A teflon bladder is incorporated in the fuel tank to provide positive expulsion in zero gravity starting. Pressurization valves are included to stop vapor diffusion through the common pressurizing line during the dormant coast period. Both propellant tanks operate at a pressure of 250 psia (for a chamber pressure of 150 psia). This pressure is required in the fuel tank to assure adequate pressure drop for regenerative cooling of the chamber. The oxidizer vapor pressure increases considerably in transit owing to the solar heating; hence, high-pressure oxidizer tankage is required. This choice of a common pressure in the tanks allows use of a single gas regulator package. Ullage settling at start is accomplished by diverting the products of a gas generator through properly oriented nozzles to provide approximately 0.04-g acceleration for 15 sec prior to main-stage ignition. The gas generator is supplied with monopropellant from the fuel tank. The system as presented here does not include an attitude control mechanism. The attitude control function could be performed by continuing monopropellant operation throughout main-stage burning and adding sufficient hot gas nozzles to accomplish this control.

In view of the high chamber temperature developed with this propellant combination (7000°F) and the highly reactive products generated, a conventional and perhaps conservative regeneratively cooled thrust chamber and radiatively cooled exhaust cone are proposed. A completely uncooled engine would necessitate the development of high strength, high-temperature materials with immunity to fluorinated products. An ablative chamber similar in mass to the cooled chamber would be expected to undergo large throat geometry changes during the stage firing owing to the extreme heating rates encountered.

The proposed chamber would be cooled by a single pass of the fuel to an expansion ratio of approximately 10:1. From this point to the full expansion, a 0.030-in. titanium skirt would be added. The choice of expansion ratio at the exit has been arbitrarily set at 40:1. This value has been selected for use in accompanying preliminary design studies and represents a practical compromise between added envelope size and impulse attainment. A detailed heat transfer analysis for a specific engine has not been conducted since necessary fuel properties are as yet unpublished. Cooling capability superior to pure hydrazine has been promised by the fuel developers.

The choice of 150-psia chamber pressure was based on expected chamber cooling limitations. Since the propellant tanks are designed to minimum gage consideration, little improvement in system mass can be accomplished by choosing a lower chamber pressure. The line drop from the fuel tank through the cooling tubes has been estimated at 30 psi, and the injector pressure drop has been estimated at 70 psi. The oxidizer line drop may be adjusted by restrictors to match that of the fuel line.

The propellant tanks chosen for this stage would both be constructed of 6A1-4V titanium. This high-strength material has proved compatible with these propellants. For a nonpreferentially oriented craft the spherical tanks employed also provide minimum tank area exposed to the solar flux. The maximum allowable design stress of this material is 135,000 psi at −210°F and 110,000 psi at 70°F. The minimum gage of tank material considered achievable in spherical tanks is 0.025 in. A design factor of 50% is included in tank calculations to account for the weight of necessary weldments, bosses, and mounts. For the oxidizer tank this factor includes necessary slosh baffles, and for the fuel tank it includes the bladder and bladder attachment accessories. The propellant densities at firing were taken to be 61.5 lb/cu ft for the fuel and 79.2 lb/cu ft for the oxidizer. The available fluorine density data at temperatures greater than −260°F were rather sketchy, and the data used are extrapolations from available information.

The helium tank is submerged in the fluorine during coast to take advantage of the low temperature. As the propellant tanks empty during firing, the helium tank is exposed to the warm incoming pressurizing gas. This allows for some warmup of residual helium and consequently a better expulsion efficiency in the helium tank. Of the helium loaded, only 88% can be utilized for propellant pumping; the rest remains in the supply tank as unavailable residual. The helium tank is constructed of 6AL-4V titanium for chemical compatibility with the fluorine. A 50% design factor was also applied to the helium tank to account for welds and fixtures. The selected design pressure is 3000 psia.

The load-carrying structure of this stage, as proposed, is illustrated in Fig. 14. The fuel tank is rigidly attached to the structure, and the thrust load from the engine

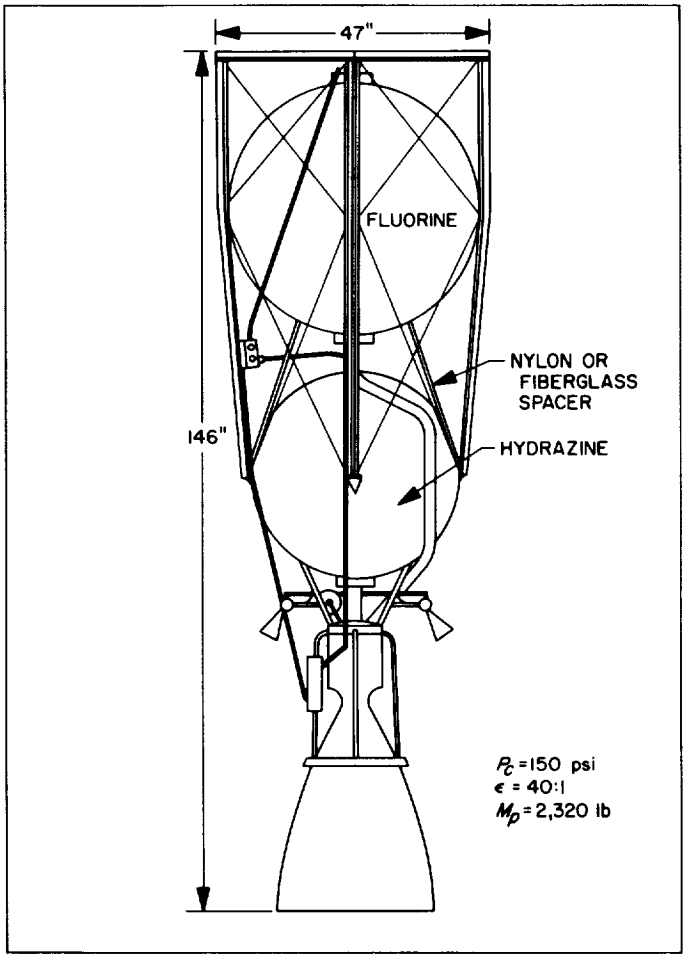

Fig. 14. Preliminary system configuration for a fluorine–hydrazine blend propulsion system

transmitted through it. The oxidizer tank must be attached to the structure with nylon or fiberglass isolators to minimize heat leaks from the spacecraft to the oxidizer, since the proposed tank insulation would not support a substantial thrust load. The structural mass, including plumbing for propellants, is estimated at 3% of the propellant mass.

The nonvented oxidizer tank of this propulsion system must be thermally isolated from the remainder of the spacecraft in order to maintain a reasonable oxidizer tank pressure level. Since the stage is not assumed to be preferentially oriented with respect to the Sun, the whole tank must be protected from the solar flux. If the fluorine is loaded at −325°F (4-psia vapor pressure) and allowed to absorb heat until the temperature rises to −250°F (170-psi vapor pressure), the resulting total heat absorption capacity of the fluid is 30.8 Btu/lb. With a final oxidizer ullage of 3.85%, this results in a maximum pressure of 250 psia at firing. From a study of cryogenic propellant storage in space, it appears that one of the several "super insulations" would probably be most practical for tank insulation. In the heat transfer analysis it has been assumed that the external surface of the insulation could be maintained at about 0°F for a trip to Mars. Therefore, the effective temperature difference across the insulation would vary from 325 to 250°F. For the purpose of this study an average of 290°F is used. The heat leak rate that can be tolerated by the oxidizer dictates the insulation requirements. For ease in computation, the heat leak due to conduction through supports has been arbitrarily assumed equal to the net solar heat absorbed by the exposed tank surface. As the time of coasting increases, the insulation requirement likewise increases since the integrated heat input is fixed by the propellant heat capacity.

The stage geometry chosen is illustrated in Fig. 14 (P_c = 150 psia). Owing to the tapered envelope, the stage would probably be oriented in a chamber-up position at launch from Earth to better fit the boost vehicle shroud enclosure. By placing the fuel tank between the oxidizer tank and the engine, the heat absorbed by the engine in space will have a longer path to travel to the low-temperature oxidizer heat sink. This orientation also minimizes conduction along the oxidizer plumbing, since the length of the oxidizer feed line is at a maximum. The oxidizer tank is partially shadowed from engine exhaust during firing by the fuel tank. If necessary, the oxidizer tank may be isolated from the payload by insulating shields at the payload-tank support interface.

The system mass for this system may be estimated by adding the propellant-scaled mass, which is a weak function of the storage time, from Fig. 15 to the thrust-scaled mass from Fig. 16 according to Eq. (1).

D. Solid-Propellant System

A description of the propulsion system employing solid propellants is presented in this section. For these motors, it is possible to derive the performance potential if the values of two general constants are known or can be assumed. These constants, needed in the payload computation, are the specific impulse and the mass ratio. The latter is defined as the mass of the burned propellant divided by the propulsion system burnout mass M_p/M_{ps}. The use of the single parameter M_p/M_{ps} to describe the burnout mass expresses the fact that the thrust-scaled mass coefficient in Eq. (1) is essentially zero for solid-propellant systems. Thus the propellant-scaled mass co-

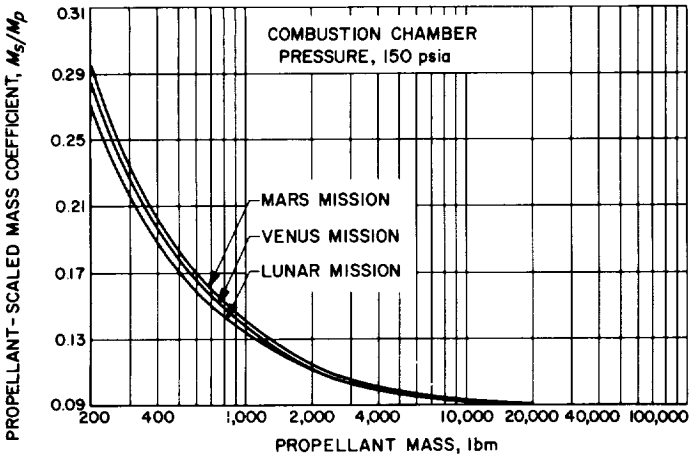

Fig. 15. Propellant-scaled mass coefficient for a fluorine–hydrazine blend bipropellant propulsion system

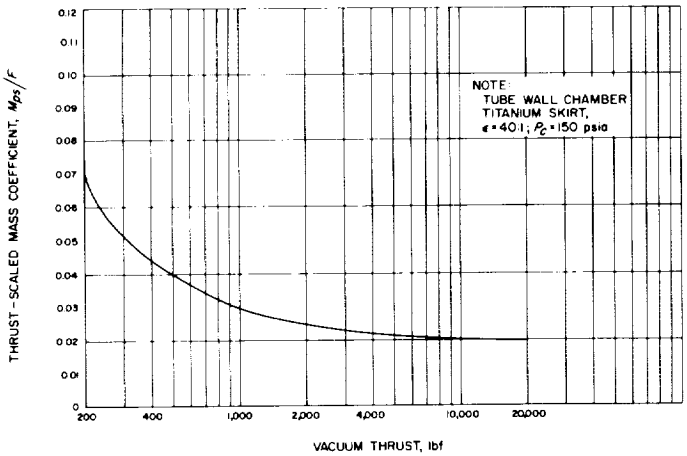

Fig. 16. Thrust-scaled mass coefficient for a fluorine–hydrazine blend bipropellant propulsion system

efficient M_s/M_p in Eq. (1) is the reciprocal of the mass ratio M_p/M_{ps}. This mass ratio is related to the propellant mass fraction ν_p by the following identity:

$$\nu_p = \frac{M_p/M_{ps}}{1 + M_p/M_{ps}} \qquad (3)$$

The system burnout mass consists of motor case, nozzle, insulation, structure, attachments, and impulse control system. When the mass of propellant required for a certain mission has been determined, use of these constants will allow the mass of the associated propulsion system and finally the payload mass to be computed. For the comparisons contained herein, specific values of the two general constants have been assumed. These values are 298 lbf-sec/lbm for the specific impulse and 18.4 for the mass ratio; the corresponding propellant mass fraction is 0.949. These performance numbers are characteristic of a solid motor only slightly more advanced than present-day technology, an assumption which is compatible with the assumptions made for the liquid systems considered. As in the case of the liquid systems, no mass allowance is included for thrust vector control.

To specify the physical characteristics of the solid-propulsion system other parameters are required, among them the effective propellant density, the attainable volume loading fraction, the size limitations, and the thrust or burning time. The volume loading fraction is the volume of the propellant divided by the total volume enclosed by the motor case. The ranges of thrust and burning time which may be conveniently obtained for a given propellant mass are illustrated in Fig. 17-20 for several values of motor case length-to-diameter ratio. Based on experimental results, it was assumed in constructing these curves that the propellant could be formulated to develop burning rates between 0.07 and 0.6 in./sec at chamber pressures between 200 and 600 psi. It was also assumed that volume loading fractions slightly in excess af 90% may be obtained. It is implied that the wide range of burning times displayed in Fig. 17-20 can be obtained with no decrement in the specific impulse or propellant mass fraction assumed in the preceding paragraph.

Sketches of two typical solid-propellant motor configurations are shown in Fig. 21. The dimensions given

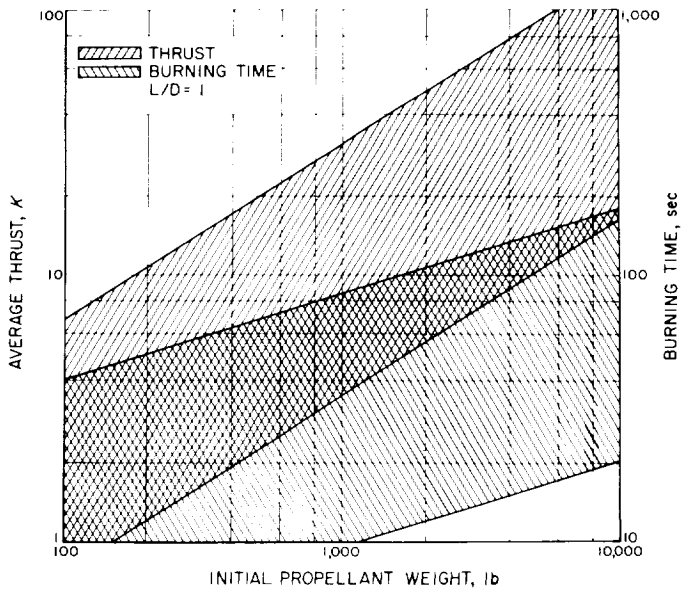

Fig. 17. Range of permissible thrust and burning time for spherical solid-propellant motors with variable propellant mass

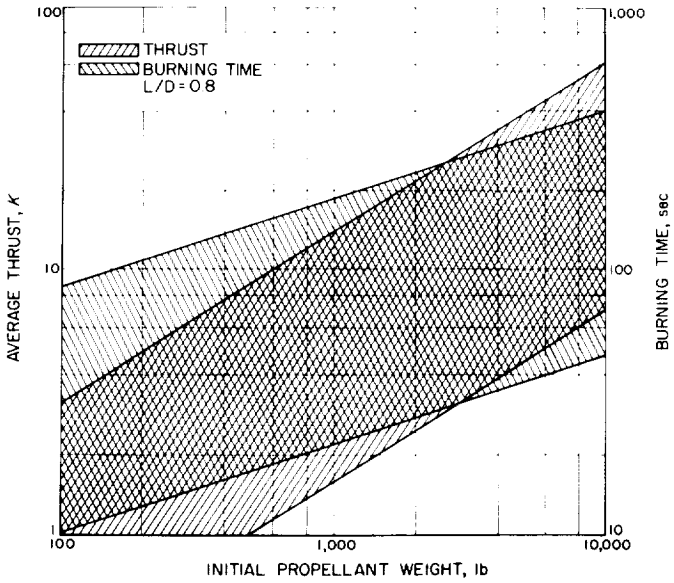

Fig. 18. Range of permissible thrust and burning time for cylindrical solid-propellant motors with variable propellant mass

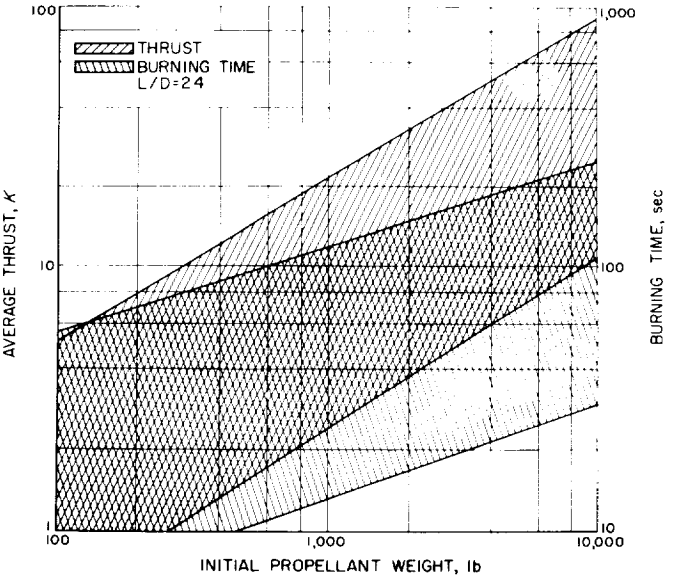

Fig. 19. Range of permissible thrust and burning time for cylindrical solid-propellant motors with variable propellant mass

correspond to propulsion systems with the same stage velocity-payload capability as that for the various liquid-propulsion systems shown in Fig. 2, 9, and 14.

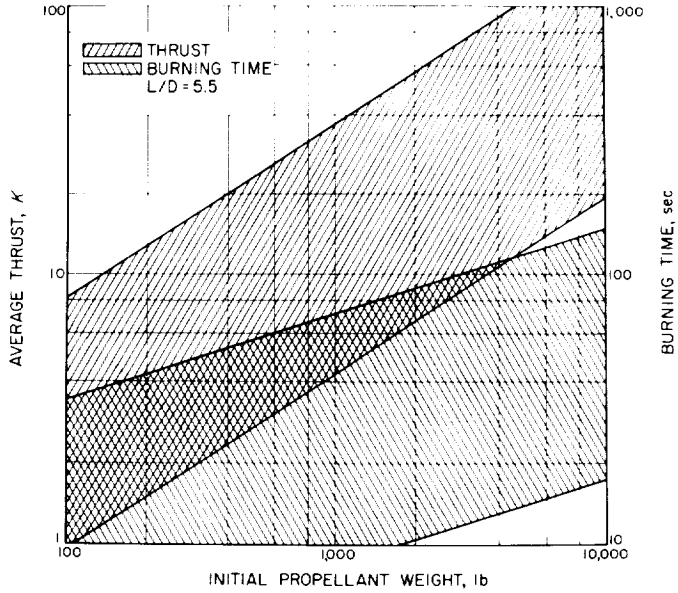

Fig. 20. Range of permissible thrust and burning time for cylindrical solid-propellant motors with variable propellant mass

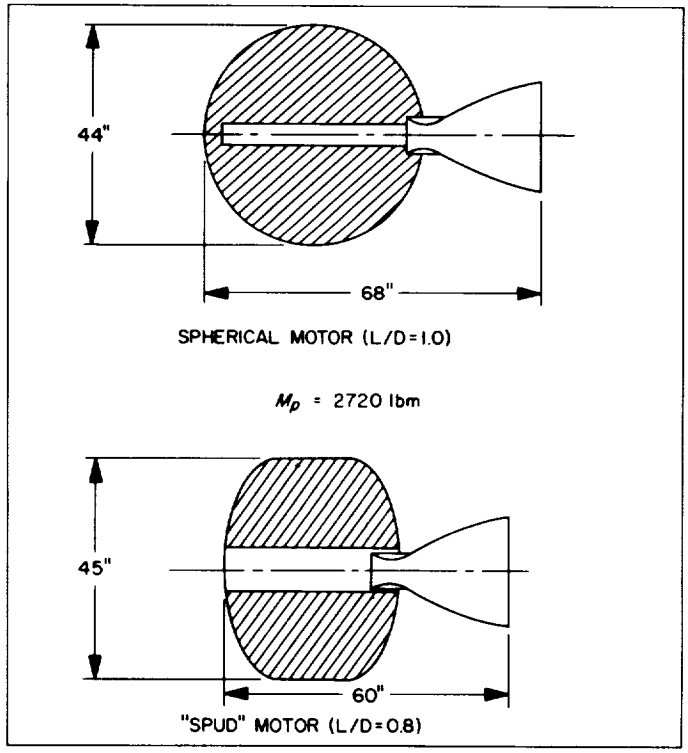

Fig. 21. Configurations of spherical and cylindrical solid-propellant motors

IV. PAYLOAD COMPARISON

This section presents comparisons of vehicle payload capabilities for selected ideal velocity increments for each of the systems described in this report. The vehicle velocity increments were selected, as indicated in Table 2, to correspond to retro missions of particular interest. The relations which define the velocity increments for these missions are given in the Appendix. For each of the velocity increments which appear in Table 2, the payload mass was computed for a range of stage gross masses between 1000 and 20,000 lb. This computation was performed as follows.

The propellant mass required was computed from the "idealized rocket equation" as follows:

$$M_p = M_g \left[1 - \exp\left(-\Delta V / I_s g_c\right)\right] \qquad (4)$$

Next, the propulsion system masses were determined for the N_2O_4–N_2H_4, O_2–H_2, F_2–N_2H_4, and solid-propellant systems using Eq. (1) and (2), as discussed in Section III. The chamber pressure selected in the determination of the scaling coefficients for the N_2O_4–N_2H_4 system was 150 psia while that for the O_2–H_2 system was 50 psia. In determining the thrust-scaled mass coefficient for all systems, it was assumed that the initial thrust-to-mass ratio was 1.0. Once the propellant and propulsion system burnout masses had been determined, the payload masses were derived from the following equation:

$$M_{pay} = M_g - M_p - M_{ps} \qquad (5)$$

The propellant, propulsion-system-burnout, and payload masses, determined for each retro mission shown in Table 2 and for each propellant system, are presented in Table 3. A graphical presentation of these results appears in Fig. 22-26 for each of the five selected velocity increments, respectively. To allow greater accuracy in comparing these curves, the payloads for each gross mass were scaled by dividing by a common denominator. The payload mass of the solid-propellant system was arbitrarily chosen for this scaling factor. The payload mass of the solid system has also been included in Fig. 22-26 so that the comparison may be made directly in terms of the payload mass for the various systems, if this is desired.

A review of the curves presented in Fig. 22-26 shows that for many of the cases considered there is not such a substantial difference in payload mass that the choice between propulsion systems can definitely be made on that basis alone. This conclusion is dependent on the range of gross masses considered and on assumed state of development as reflected in the various propulsion system mass curves. If somewhat larger gross masses were to be considered, turbopumps could be used to pump the liquid propellants, and these systems would then probably show a somewhat greater payload advantage over the solids. Also, it is felt that the payload performances of the O_2–H_2 and/or F_2–N_2H_4 systems could be more readily improved with additional development effort than the already highly developed solid or N_2O_4–N_2H_4 systems. Thus it may be concluded that other factors such as cost, availability, reliability, and compatibility with spacecraft requirements will probably exert a greater influence on the choice of spacecraft propulsion systems than will performance considerations.

The foregoing conclusion must be tempered by the knowledge that quite often a large portion of the gross payload mass is taken up by systems other than the propulsion system. Systems such as power supply, communications, guidance, structure, and life support are included in this category. Often, a relatively small percentage difference in over-all or gross payload capacity may result in a substantial difference in net or scientific payload. Under these conditions, a small improvement in propulsion system performance may allow a marginal mission to be completed with existing boost vehicles. Therefore, performance may at times be the overriding consideration.

Two additional conclusions may be drawn from this study:

1. There is very little difference in payload performance between the solid and N_2H_4–N_2O_4 liquid systems. The constant mass ratio used for the solid system yields a lighter system than the storable liquid combination at the lower gross masses. As the gross mass increases, the specific impulse advantage of the liquid system and the decreasing mass scaling coefficients yield propulsion systems which are lighter than the solid system.
2. The O_2–H_2 system may be employed most effectively for lunar missions since the effects of storage time on the resultant system masses are relatively low for these missions. However, for the missions to Venus and Mars, the F_2–N_2H_4 system appears to be somewhat better than O_2–H_2 because the former system is substantially less sensitive to the length of the storage period in space.

Table 2. Description of mission considered

Figure	Velocity increment, fps	Storage time, days	Retro mission	Notes
22	3,000	3	(a) Circular lunar orbit @ 50 to 500 mi (b) Highly elliptical, lunar orbit periapsis, 50 to 500 mi apoapsis, 10,000 mi	(a) 66-hr lunar transfer trajectory (b) 42-hr lunar transfer trajectory Orbit altitude (a) or periapsis altitude (b) depends on position of Moon at launch
23	6,500	150 300	Highly elliptical Venusian orbit periapsis, 100-1000 mi apoapsis, 10,000 mi Highly elliptical Martian orbit periapsis, 100 mi apoapsis, 10,000 mi	Applies during years when the planetary approach velocities are relatively low (Venus 1967, Mars 1962)
24	8,750	3 150	Lunar direct-descent, soft-landing vehicle Highly elliptical, Venusian orbit periapsis, 100 mi apoapsis, 10,000 mi	66-hr lunar transfer trajectory Allows the highly elliptical Venusian orbits to be attained in less favorable years (1962, 1965, 1970)
25	10,500	3 150 300	Lunar soft lander with elliptical transfer descent from circular parking orbit Elliptical Venusian orbit periapsis, 100 mi apoapsis, 3600 mi Elliptical Martian orbit periapsis, 100 mi apoapsis, 2500 mi	66-hr lunar transfer trajectory These elliptical orbits may be attained in the less favorable launch opportunities (i.e., those with high approach velocities)
26	14,000	150 300	Circular Venusian orbit @ 100 to 1000 mi Circular Martian orbits @ 100 mi or lower	The Venusian orbits may be attained except during the more unfavorable launch opportunities. The Martian orbits may be attained at any encounter. A ΔV of this magnitude is quite conservative for the Mars orbiter mission

Table 3. System mass comparison

ΔV fps	M_g lb	N_2O_4–N_2H_4			O_2–H_2							F_2–N_2H_4							Solid		
		Storage time,[a] days																			
		3, 150, 300				3		150		300			3		150		300		3, 150, 300		
		M_p lb	M_{ps} lb	M_{pay} lb	M_p lb	M_{ps} lb	M_{pay} lb	M_{ps} lb	M_{pay} lb	M_{ps} lb	M_{pay} lb	M_p lb	M_{ps} lb	M_{pay} lb	M_{ps} lb	M_{pay} lb	M_{ps} lb	M_{pay} lb	M_p lb	M_{ps} lb	M_{pay} lb
3,000	1,000	255	50	695	195	109	696					219	86	695					268	15	717
	2,000	510	82	1,408	390	173	1,437					438	128	1,434					536	29	1,435
	5,000	1,275	166	3,559	975	317	3,708					1,095	249	3,656					1,340	73	3,587
	10,000	2,550	296	7,154	1,950	507	7,543					2,190	439	7,371					2,680	146	7,174
	15,000	3,825	420	10,755	2,925	681	11,394					3,285	637	11,078					4,020	219	10,761
	20,000	5,100	542	14,358	3,900	851	15,249					4,380	821	14,799					5,360	291	14,349
6,500	1,000	471	68	461	375			341	284	455	170	414			109	477	112	474	492	27	481
	2,000	942	116	942	750			480	770	624	626	828			171	1,001	174	998	984	53	963
	5,000	2,355	248	2,397	1,875			750	2,325	944	2,181	2,040			337	2,623	341	2,619	2,460	134	2,406
	10,000	4,710	452	4,838	3,750			1,105	5,145	1,352	4,898	4,060			602	5,338	610	5,330	4,920	267	4,813
	15,000	7,065	651	7,284	5,625			1,430	7,945	1,703	7,672	6,080			876	8,044	882	8,038	7,380	401	7,219
	20,000	9,420	846	9,734	7,500			1,760	10,740	2,068	10,432	8,100			1,145	10,755	1,158	10,742	9,840	535	9,625
8,750	1,000	576	77	347	468	175	357	377	155			514	116	370	120	366			598	33	369
	2,000	1,152	132	716	936	271	793	527	537			1,028	185	787	189	783			1,196	65	739
	5,000	*2,880	286	1,834	2,340	482	2,178	827	1,833			2,570	382	2,048	382	2,048			2,990	163	1,847
	10,000	5,760	528	3,712	4,680	810	4,510	1,246	4,074			5,140	696	4,164	696	4,164			5,980	325	3,695
	15,000	8,640	760	5,600	7,020	1,131	6,849	1,635	6,345			7,710	1,019	6,271	1,019	6,271			8,970	488	5,542
	20,000	11,520	992	7,488	9,360	1,433	9,207	1,975	8,665			10,280	1,338	8,382	1,338	8,382			11,960	650	7,390
10,500	1,000	642	82	276	532	188	280	400	68	530	−62	579	123	298	126	295	129	292	665	36	299
	2,000	1,284	142	574	1,064	290	646	557	379	718	218	1,158	197	645	201	641	202	640	1,330	72	598
	5,000	3,210	310	1,480	2,660	520	1,820	883	1,457	1,098	1,242	2,895	409	1,696	409	1,696	415	1,690	3,325	181	1,494
	10,000	6,420	573	3,007	5,320	872	3,808	1,326	3,354	1,603	3,077	5,790	753	3,457	753	3,457	762	3,448	6,650	361	2,989
	15,000	9,630	831	4,539	7,980	1,230	5,790	1,752	5,268	2,075	4,945	8,685	1,102	5,213	1,102	5,213	1,115	5,200	9,975	542	4,483
	20,000	12,840	1,080	6,080	10,640	1,577	7,783	2,152	7,208	2,492	6,868	11,580	1,452	6,968	1,452	6,968	1,469	6,951	13,300	723	5,977
14,000	1,000	746	90	164	636			432	−68	531	−167	684			137	179	140	176	768	42	190
	2,000	1,492	158	350	1,272			597	131	764	−36	1,368			222	410	223	409	1,536	83	381
	5,000	3,730	348	922	3,180			952	868	1,179	641	3,420			455	1,125	464	1,116	3,840	209	951
	10,000	7,460	648	1,892	6,360			1,466	2,174	1,689	1,951	6,840			843	2,317	857	2,303	7,680	417	1,903
	15,000	11,190	940	2,870	9,540			1,945	3,515	2,280	3,180	10,260			1,242	3,498	1,258	3,482	11,520	626	2,854
	20,000	14,920	1,230	3,850	12,720			2,440	4,840	2,802	4,478	13,680			1,637	4,683	1,651	4,669	15,360	835	3,805

[a] Nominal storage times: 3 days, lunar retro missions; 150 days, Venusian retro missions; 300 days, Martian retro missions.

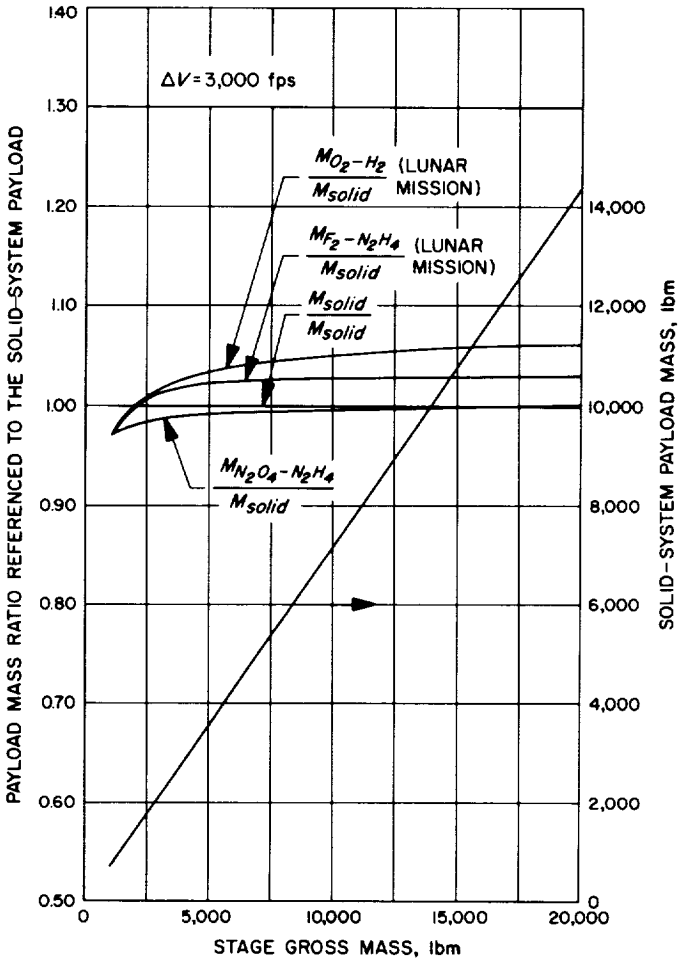

Fig. 22. Payload mass ratios and solid-system payload mass as functions of stage gross mass

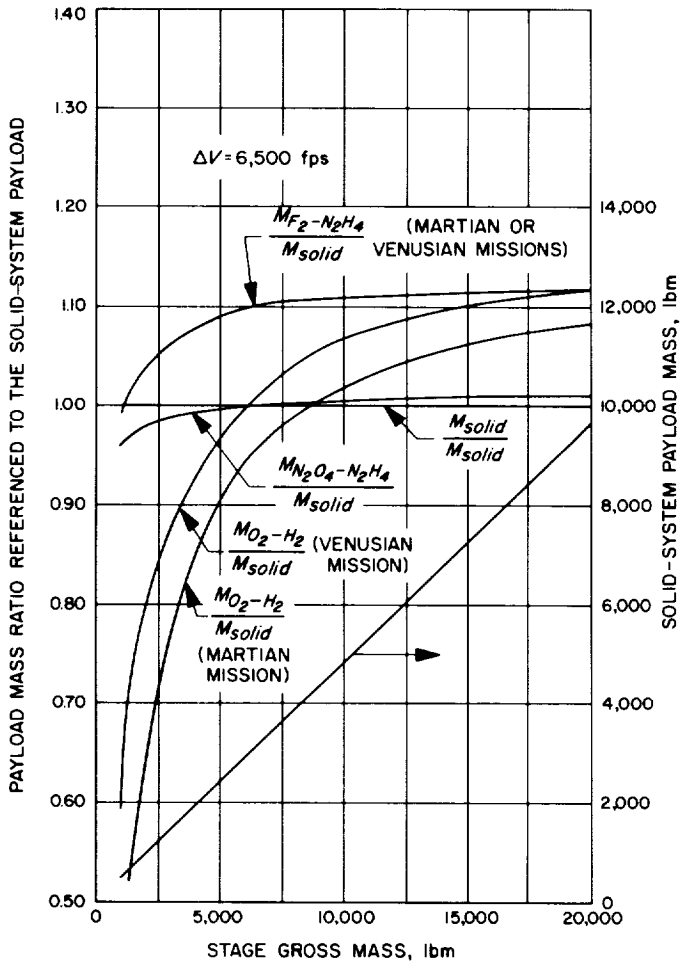

Fig. 23. Payload mass ratios and solid-system payload mass as functions of stage gross mass

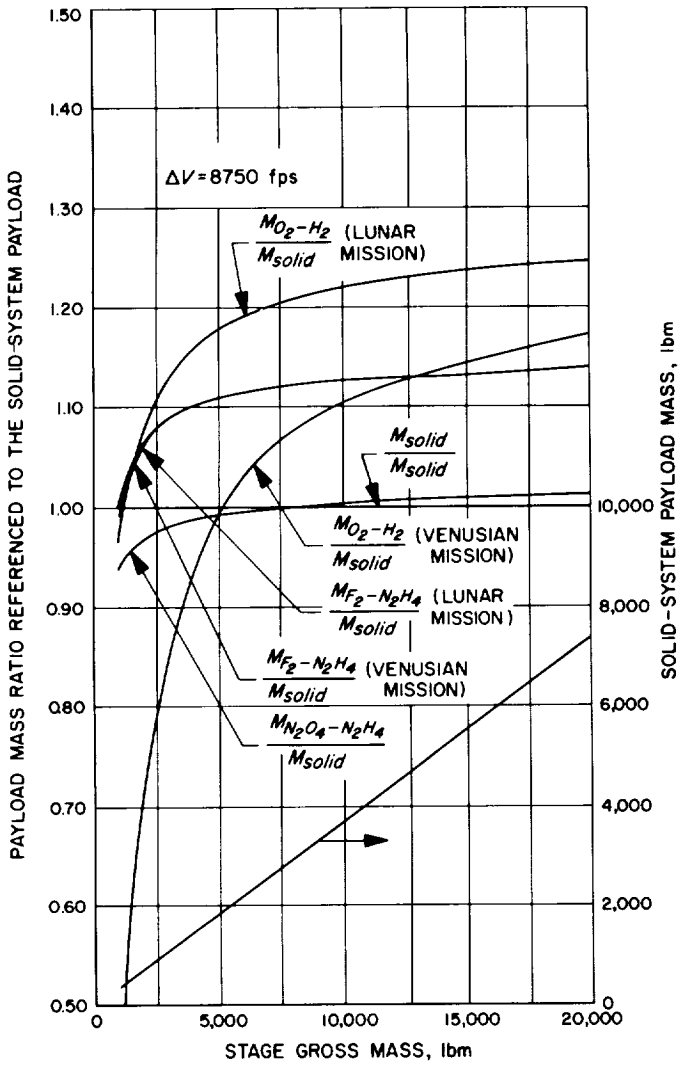

Fig. 24. Payload mass ratios and solid-system payload mass as functions of stage gross mass

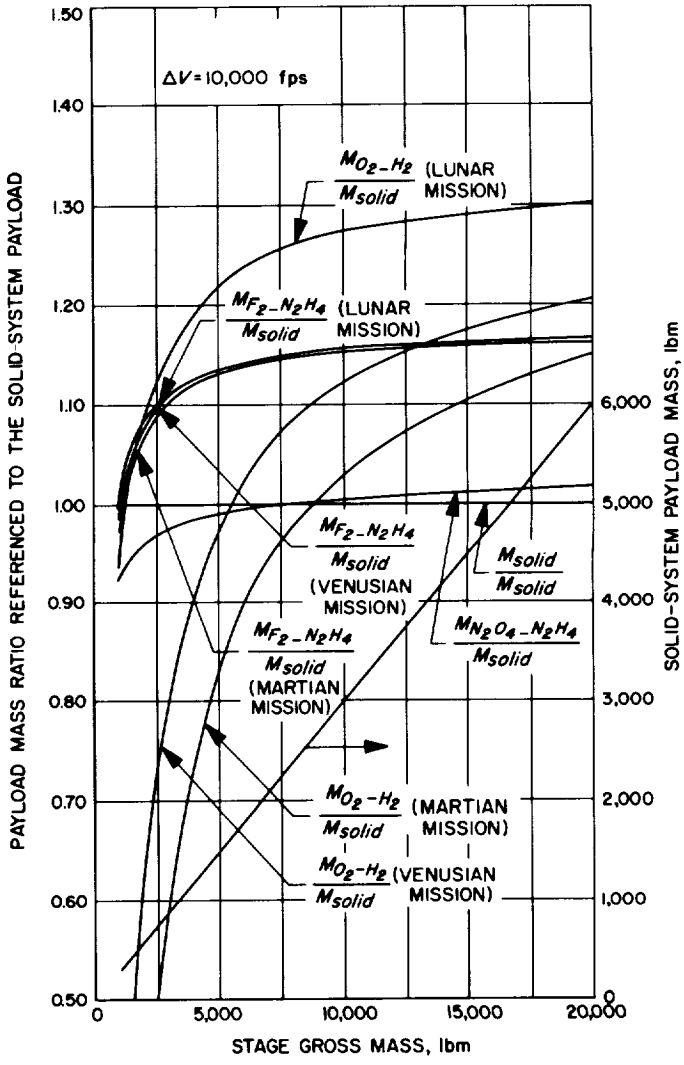

Fig. 25. Payload mass ratios and solid-system payload mass as functions of stage gross mass

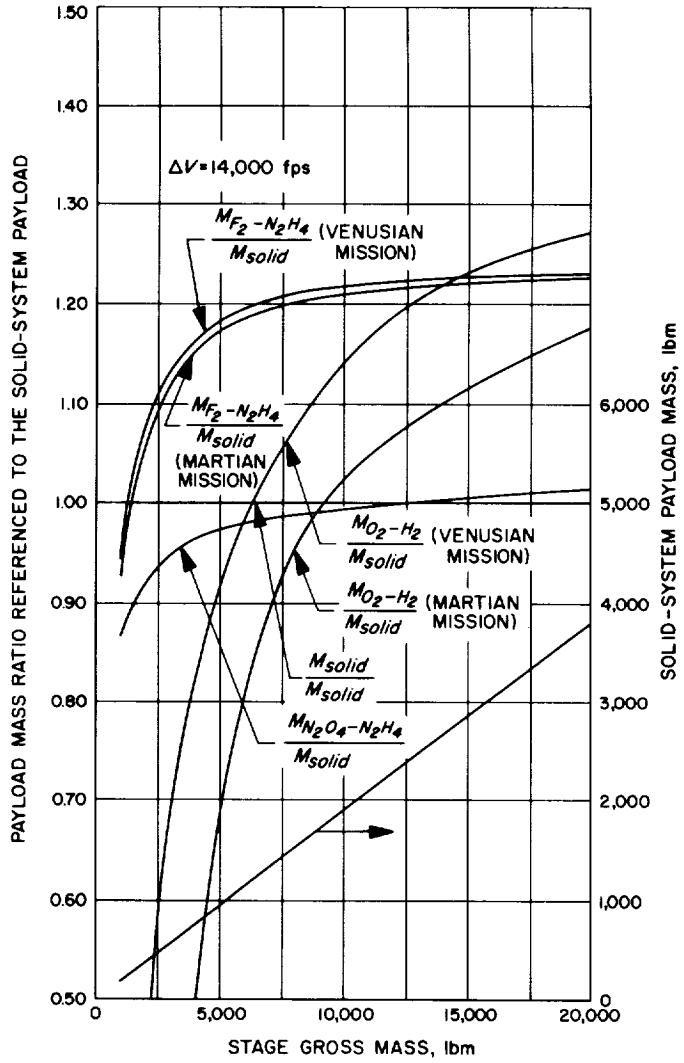

Fig. 26. Payload mass ratios and solid-system payload mass as functions of stage gross mass

APPENDIX

Velocity Increment Requirements

The discussion here concerns velocity increments which may be required of the propulsion systems for retro operations. The two types of missions considered are (1) establishing an orbit around the Moon, Venus or Mars, and (2) slowing a vehicle to soft-land on the Moon. Landing missions on Mars or Venus are not considered since heat shield mass estimates for aerodynamic-drag braking (Ref. 8) yield payload mass estimates 2 to 20 times larger than those resulting from the use of retrorocket braking. Lunar missions are considered in Section I; planetary missions are considered in Section II. Methods of analysis follow procedures developed in Ref. 9. Extensive use is made of the parameter V_∞, the hyperbolic excess velocity relative to a celestial body. This is the actual velocity which a vehicle would possess in the vicinity—but outside the gravitational influence—of the subject body.

I. LUNAR MISSIONS

The lunar missions will be discussed in the following order: landing missions, circular orbits, and elliptical orbits. The hyperbolic excess velocity relative to the Moon as a function of the Earth–Moon transit time is illustrated in Fig. A-1. It may be observed that two curves are obtained owing to the eccentricity of the Moon's orbit around the Earth. The actual flight time would fall somewhere between these extremes, depending upon the relative position of the Moon at the time of arrival.

The velocity decrement required for a direct descent to a soft landing will be treated first. For a single retro impulse applied instantaneously just prior to impact with the Moon's surface, the required velocity decrement may be calculated from the following equation:

$$\Delta V_{DD} = \left[V_\infty^2 + \frac{2\mu}{r_b} \right]^{1/2} \qquad \text{(A-1)}$$

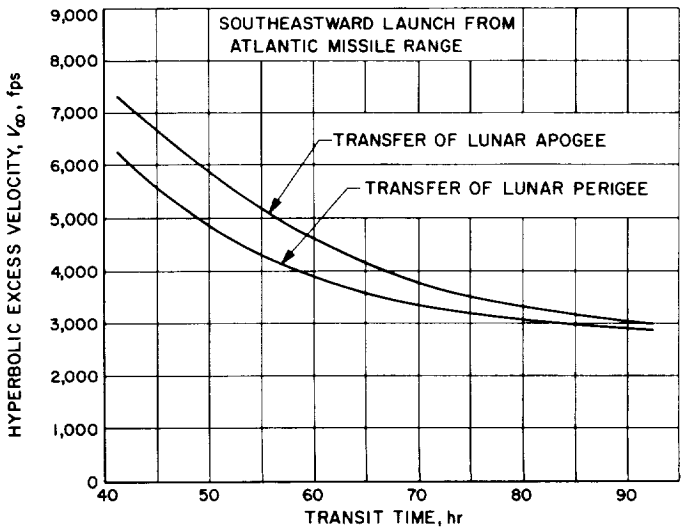

Fig. A-1. Hyperbolic excess velocity relative to the Moon for Earth–Moon transfers

The lunar characteristic constants used in this equation are:

$$\mu = 1.7270 \times 10^{14} \text{ ft}^3/\text{sec}^2$$

$$r_b = 1{,}080 \text{ mi} = \text{lunar radius}$$

This expression is plotted as the $h = 0$ curve in Fig. A-2 for the range of hyperbolic excess velocities of interest. For the finite burning times of interest, the velocity decrements actually required will be somewhat greater than those shown in Fig. A-2 (up to 200 ft/sec). Since this correction is small compared to ΔV_{DD}, the latter will be used alone as being representative of the actual requirements for purposes of the present comparisons. A discussion of the gravity-burning time effects on velocity requirements for direct-descent vehicles is available in Ref. 10.

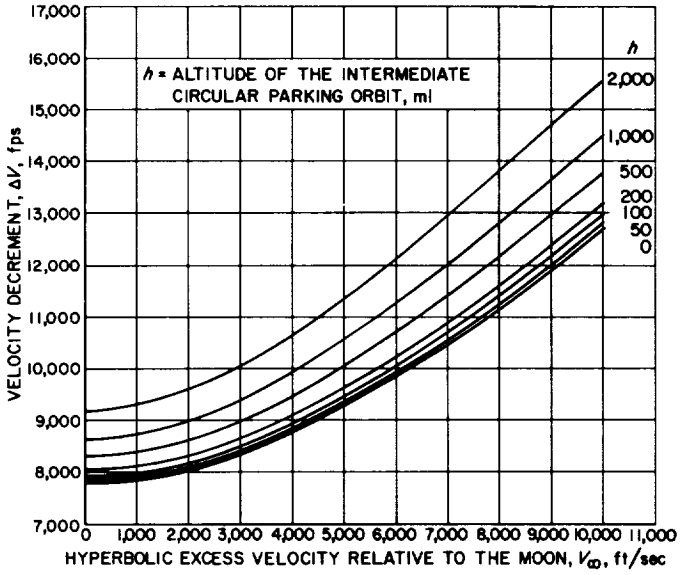

Fig. A-2. Velocity decrement requirements for lunar parking orbits with elliptical transfer descent

Another idealized method of descent to the lunar surface would be to establish the spacecraft in a circular parking orbit by applying an impulsive velocity decrement at the periapsis of a miss trajectory. After choosing a landing area, descent from the parking orbit would be accomplished via an elliptical transfer descent. This is accomplished by applying a retro impulse to establish an elliptical transfer path to the lunar surface. As the lunar surface is approached, a second retro impulse is applied to bring the vehicle to rest. The advantage of the parking orbit method is that a greater degree of selectivity may be exercised in choosing the landing area.

The required total velocity increment for the three impulses involved in this maneuver is given by:

$$\Delta V_{ET} = \left[V_\infty^2 + \frac{2\mu}{r_o}\right]^{1/2} + \left(\frac{2\mu}{r_o + r_b}\right)^{1/2} \left[\frac{1 - r_b/r_o}{(r_b/r_o)^{1/2}}\right] \quad \text{(A-2)}$$

This expression has been evaluated for a range of parking orbit altitudes up to 2000 mi, and the results are plotted in Fig. A-2. These curves show that the parking orbit method requires increasingly more total vehicle velocity requirement than the direct descent as the altitude of the parking orbit increases. Here again the effects of the finite burning times to be used would increase the effective velocity requirements somewhat (on the order of 50 ft/sec or less); however, this simplified treatment will suffice for the comparisons to be made.

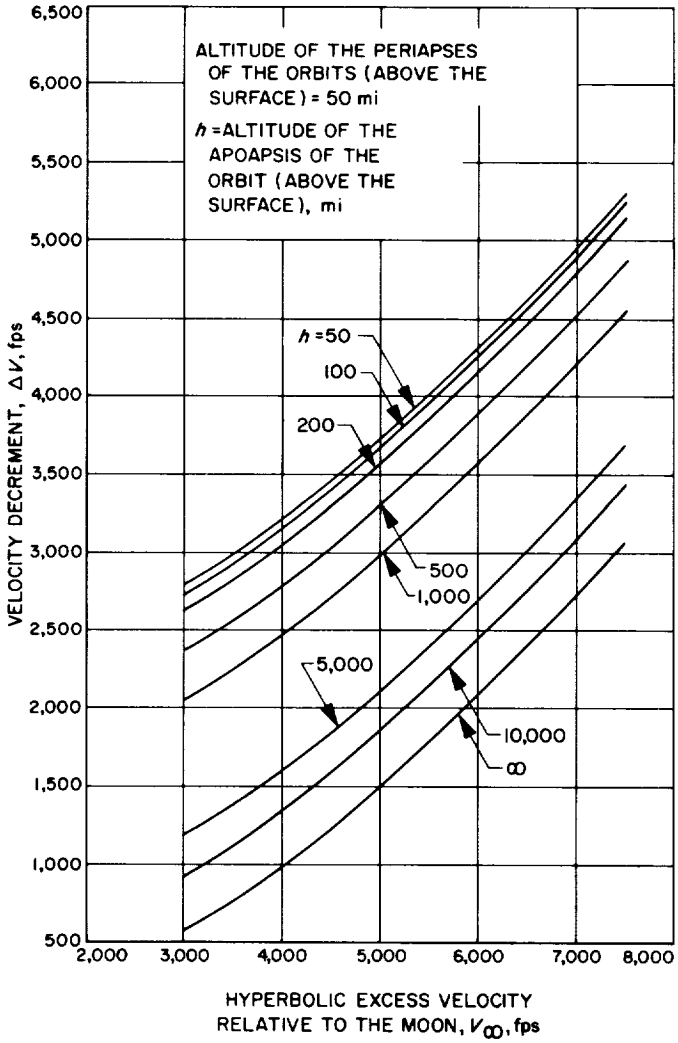

Fig. A-3. Velocity decrement required for attainment of elliptical lunar orbits

Next to be considered is the case where the desired objective is to place the spacecraft into an orbit around the Moon. For the case of a circular orbit, the following equation may be used to find the required velocity decrements:

$$\Delta V_{CO} = \left[V^2 + \frac{2\mu}{r_o}\right]^{1/2} - \left(\frac{\mu}{r_o}\right)^{1/2} \qquad \text{(A-3)}$$

The maneuver implied in this case is that described in the preceding paragraph for establishment of the parking orbit. Velocity decrements were computed by Eq. (A-2) for circular orbit altitudes up to 500 miles for each of three hyperbolic excess velocities and are presented as the curves of $r_o = r_p$ in Fig. A-3, A-4, and A-5. If attainment of an elliptic orbit will satisfy mission objectives, the velocity decrements may be substantially decreased. In this case, the decrement may be computed from the following equation:

$$\Delta V_{EO} = \left[V_\infty^2 + \frac{2\mu}{r_p}\right]^{1/2} - \left[\frac{2\mu r_a}{r_p\,(r_a + r_p)}\right]^{1/2} \qquad \text{(A-4)}$$

This expression has been evaluated as a function of V_∞ for periapsis altitudes of 50, 100, and 500 miles and apoapsis altitudes ranging from the periapsis altitude to infinity. The resultant curves are presented in Fig. A-3, A-4, and A-5, respectively.

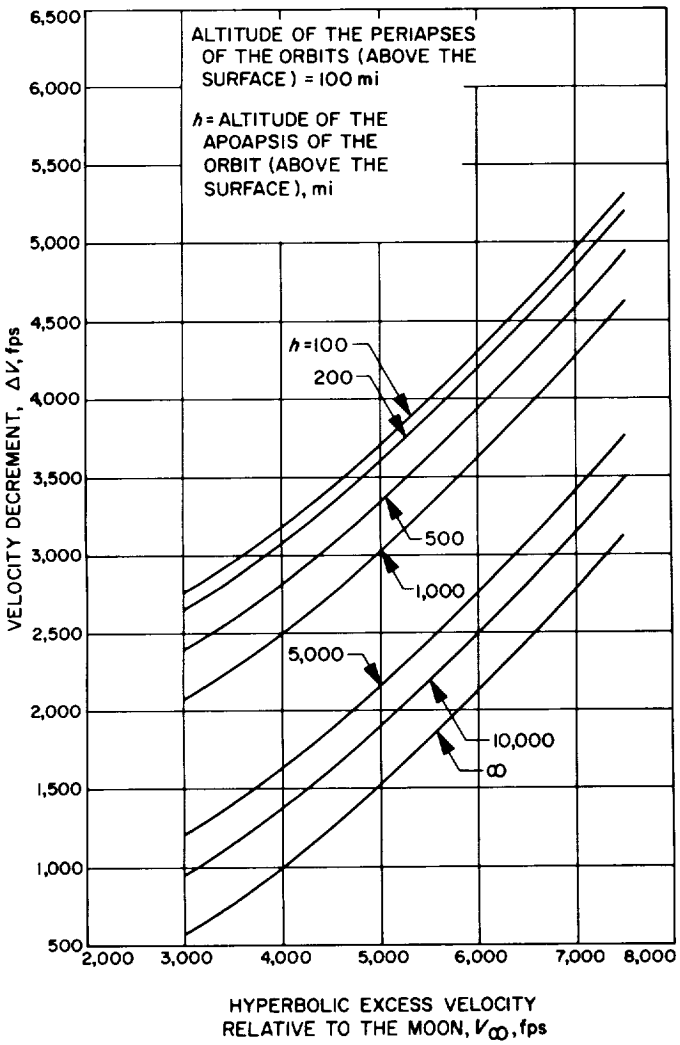

Fig. A-4. Velocity decrement required for attainment of elliptical lunar orbits

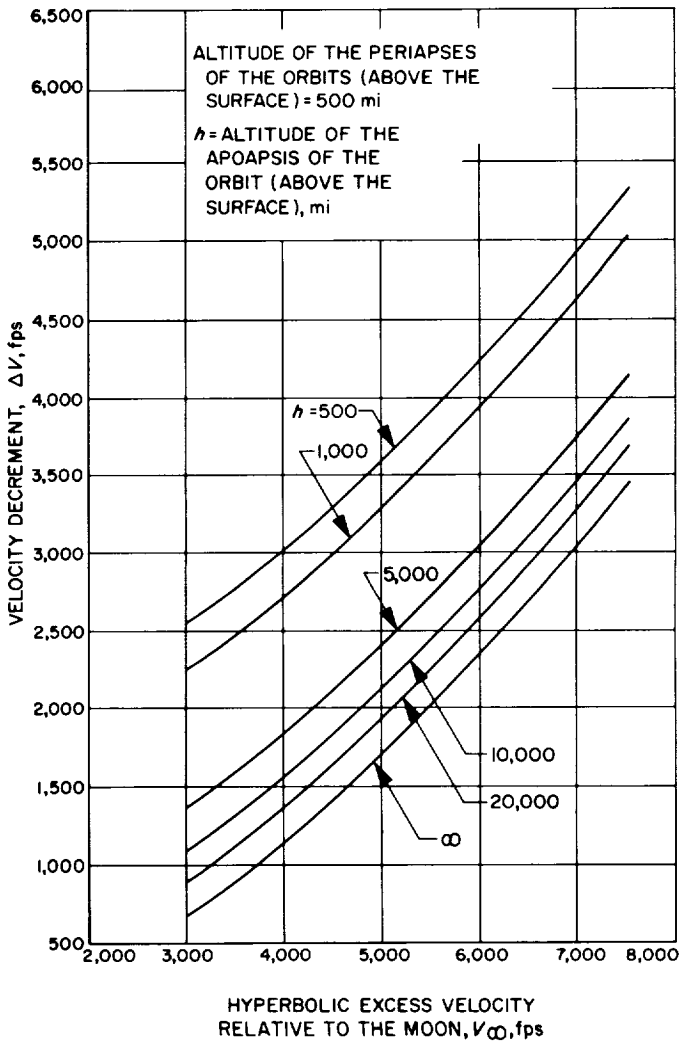

Fig. A-5. Velocity decrement required for attainment of elliptical lunar orbits

II. PLANETARY MISSIONS

This section presents a discussion of the requirements for a retro propulsion system to establish a vehicle in orbit around Mars or Venus. The values of the geophysical constants used for these calculations were abstracted from Ref. 9 and are shown in Table A-1.

Table A-1. Planetary constants

Planet	r_b, mi	μ, ft^3/sec^2
Venus	3855	1.14499×10^{16}
Mars	2057	1.51520×10^{15}

As in the lunar case, the velocity requirements for retro into planetary orbits are a function of the transfer trajectory from Earth. A detailed discussion of the possible transfer trajectories and the tradeoffs which must be made during their selection is beyond the scope of this report. For a more complete treatment, Ref. 11 or 12 may be consulted. However, it is felt that the following brief discussion may be of value. Some of the factors which must be considered in choosing planetary transit trajectories are boost energy requirements, planetary approach velocity, communication distance, and firing period. The firing period is the allowable interval during which the vehicle must be launched. Increasing the duration of the period generally means that the propellant loading must be increased, with a corresponding reduction of the payload mass. A launch interval of two to five weeks is commonly budgeted for the firing period to allow for such factors as scheduling problems and launching holds.

In the idealized case (coplanar, circular orbits), the minimum boost-energy trajectory is unique. However, results calculated by JPL's Interplanetary Trajectory Program are available. These results take account of the many variations from the ideal which characterize the actual case. As a result, the minimum boost-energy trajectory varies with the launch year. This variation is illustrated in Table A-2 for launch opportunities which occur during this decade.

Very often, consideration of the factors mentioned previously will dictate that a trajectory be employed which is somewhat different from the minimum boost energy trajectory. For instance, if an orbiting retro maneuver is to be accomplished or if the vehicle is to enter the target planet's atmosphere, it would be desirable to minimize the approach velocity. Therefore, an extensive trajectory study is usually required to establish optimum trajectory parameters. Trajectory parameters chosen from the results of such a study for the 1964 opportunities to launch toward Venus and Mars are presented in Table A-3.

Table A-2. Minimum boost-energy trajectory parameters

Planet	Year	Minimum boost-energy parameter, $ft^2/sec^2 \times 10^{-6}$	Transit time, days	Planetary approach velocity, fps
Venus	1961	0.842	125	
	1962	0.938	114	17,100
	1964	1.329	112	19,680
	1965	1.415	108	15,460
	1967	0.700	142	10,560
	1969	0.831	120	
	1970	0.916	116	17,750
Mars	1962	1.624	232	12,980
	1964	0.965	244	13,500
	1967	0.979	202	17,910
	1969	0.949	178	

Table A-3. Venusian and Martian trajectory parameters for 1964

Planet	Firing window	Boost energy parameter $ft^2/sec^2 \times 10^{-6}$	Transit time, days	Approach velocity, fps
Venus	2 weeks	1.548	232-246	15,690 to 16,880
Mars	2 weeks	1.076	104-121	13,520 to 13,790

Comparison of these results with those for the minimum energy trajectories (Table A-2) shows that the actual requirements are 12 and 16% higher for Mars and Venus, respectively. However, the resultant approach velocities are 14% lower (Venus) or about the same (Mars), and allowance has been made for a two-week firing window, whereas the minimum energy trajectory was restricted to launching during a very short interval.

The required velocity increments for the retro into orbit can be calculated from Eq. (A-3) using the constants presented in Table A-1. Results of calculations made for three periapsis altitudes and a range of hyperbolic excess velocities and apoapsis altitudes are presented in Fig. A-6, A-7, and A-8 for the Martian case and in Fig. A-9, A-10, and A-11 for the Venusian orbits. The

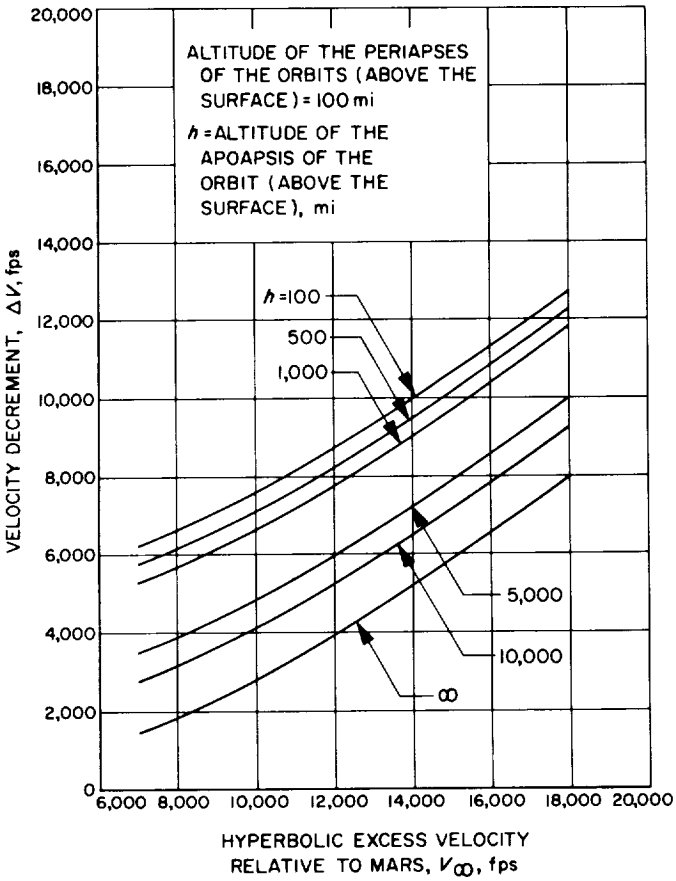

Fig. A-6. Velocity decrement required for attainment of elliptical Martian orbits

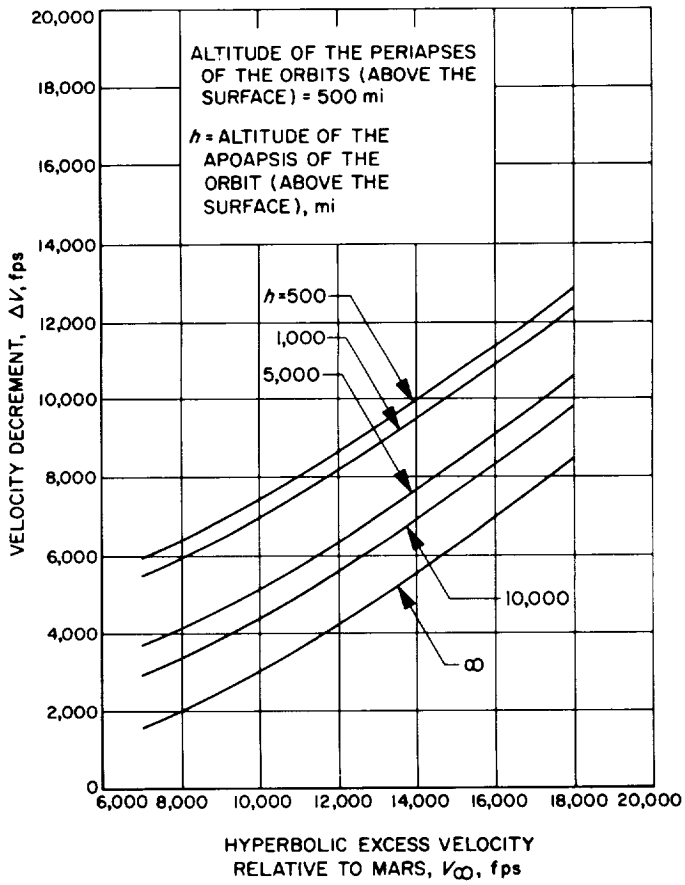

Fig. A-7. Velocity decrement required for attainment of elliptical Martian orbits

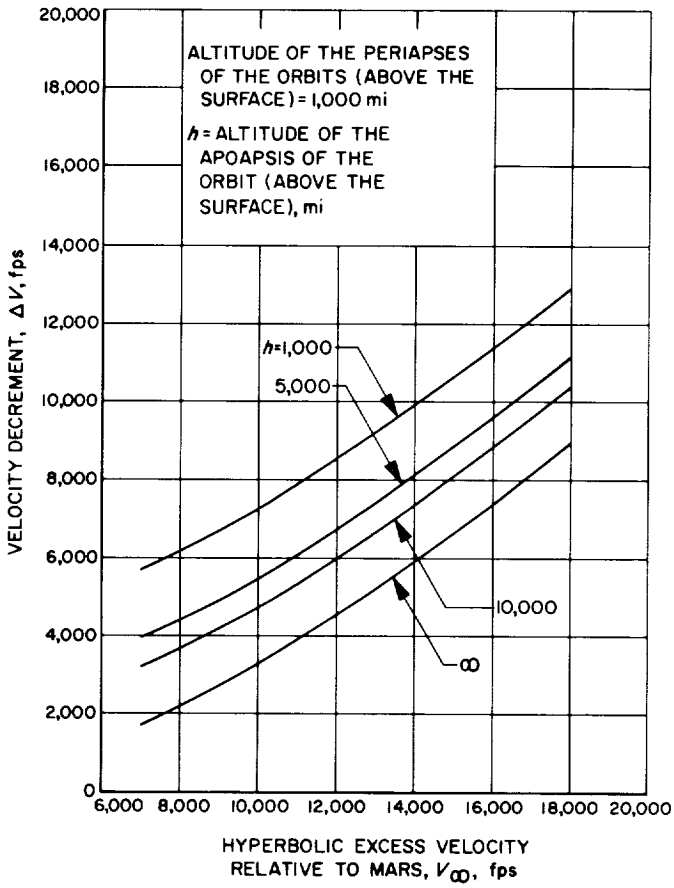

Fig. A-8. Velocity decrement required for attainment of elliptical Martian orbits

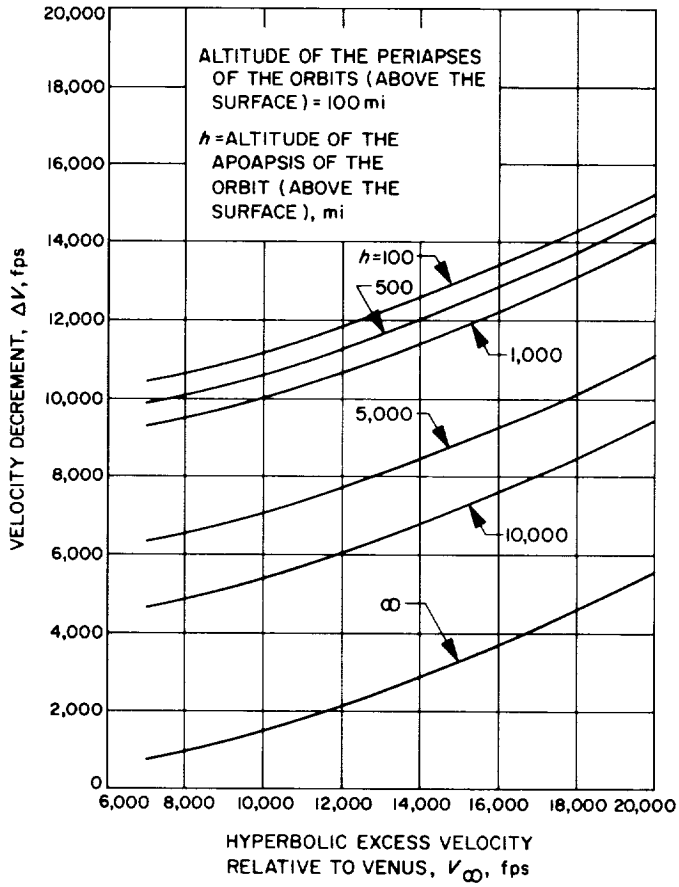

Fig. A-9. Velocity decrement required for attainment of elliptical Venusian orbits

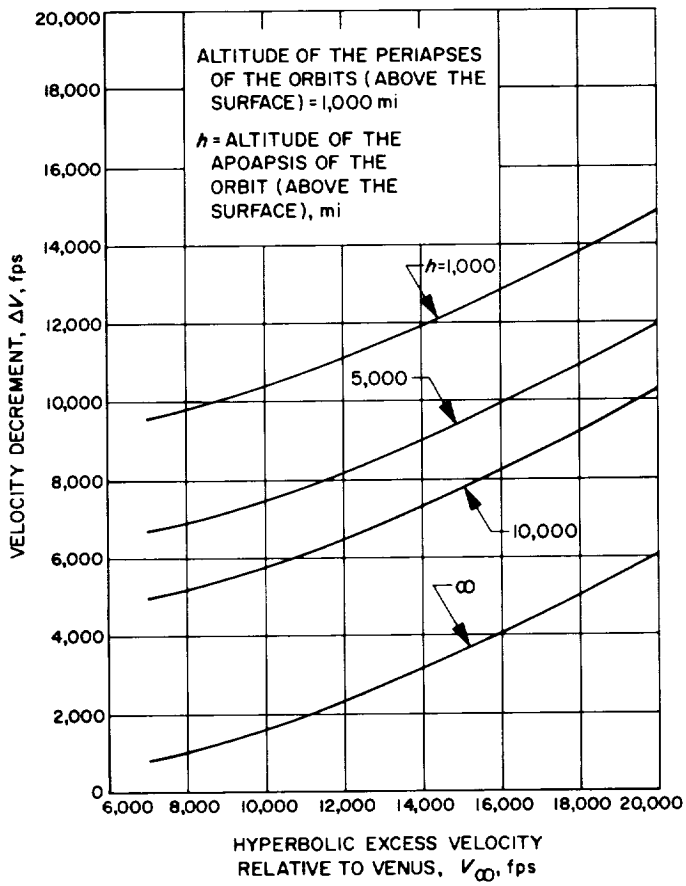

Fig. A-11. Velocity decrement required for attainment of elliptical Venusian orbits

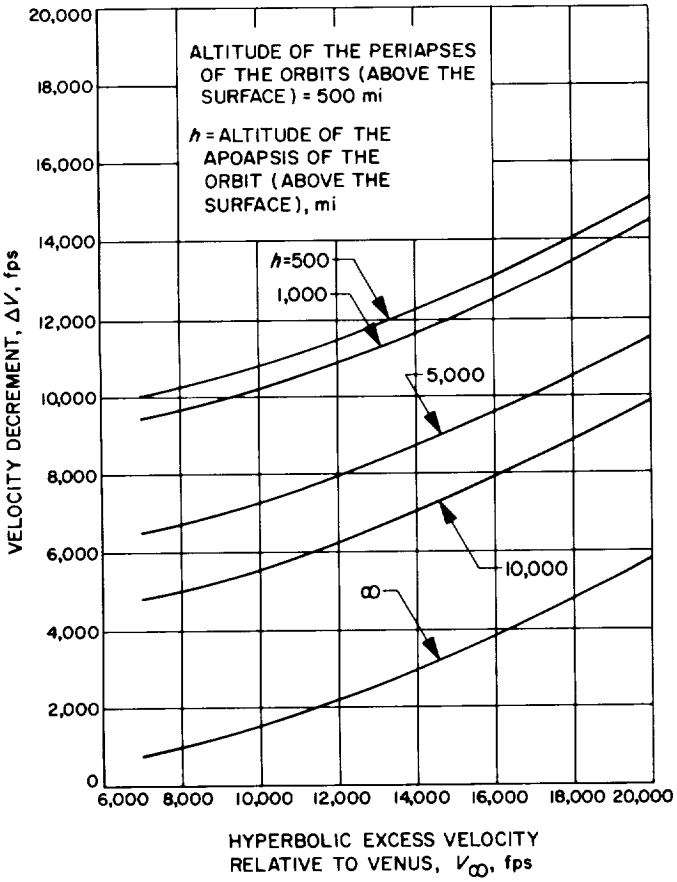

Fig. A-10. Velocity decrement required for attainment of elliptical Venusian orbits

remarks made previously in Section I concerning the gravity-burning time loss for entry into orbit are also applicable in this case. For example, in the preliminary design study of two orbiting missions around the planet Mars presented in Ref. 1, the gravity-burning time loss was estimated at only 30 ft/sec for a mission whose impulsive velocity increment was 14,500 ft/sec and 20 ft/sec for a mission which had a 7,500-ft/sec impulsive velocity increment. Therefore, the velocity increments appearing in the above figures may be used with negligible error.

NOMENCLATURE

F	thrust, lbf
g_c	constant relating force and mass in English engineering unit system, 32.174 ft/sec^2
I_s	specific impulse, lbf-sec/lbm
M_f	thrust-dependent portion of the propulsion system burnout mass, lbm
M_g	total mass prior to retrorocket ignition, lbm
M_{if}	mass of the insulation fraction of M_s, lbm
M_p	burned propellant mass, lbm
M_{pay}	payload mass, lbm
M_{ps}	propulsion system burnout mass, lbm
M_s	portion of the propulsion system burnout mass which is a function of the propellant mass, lbm
M_{sf}	mass of the pumping and tankage system fraction of M_s, lbm
P_c	thrust chamber pressure, psi
r_a	radius of the apoapsis of the orbit, mi
r_b	radius of the celestial body, mi
r_o	radius of the circular orbit, mi
r_p	radius of the periapsis of the orbit, mi
t_b	burning time, sec
V_∞	hyperbolic excess velocity, fps
ν_p	propulsion system mass fraction (defined by Eq. 3)
μ	gravitational parameter, ft^3/sec^2
ΔV	velocity increment, fps
ΔV_{CO}	velocity increment required to achieve a circular orbit, fps
ΔV_{DD}	velocity increment required for direct descent to the lunar surface, fps
ΔV_{ET}	velocity increment required for elliptic descent to the lunar surface from intermediate parking orbit, fps
ΔV_{EO}	velocity increment required to achieve an elliptic orbit, fps

REFERENCES

1. Lee, D. H., R. R. Breshears, A. D. Harper, and J. R. Wrobel, *Applications for Monopropellants in Space Vehicles,* Technical Report No. 32-174, Jet Propulsion Laboratory, Pasadena, Calif., October 5, 1961 (CONFIDENTIAL).
2. *Research Summary No. 36-7,* Volume II, Jet Propulsion Laboratory, Pasadena, Calif., March 1, 1961, pp. 36–40.
3. *Hylas,* Report SY60042, Aerojet-General Corp., Azusa, Calif., November 1, 1960 (CONFIDENTIAL).
4. *Hylas Star,* Report SY61003, Aerojet-General Corp., Azusa, Calif., November 1, 1960 (CONFIDENTIAL).
5. Olson, T., *Recombination and Condensation Processes in High-Area-Ratio Nozzles,* American Rocket Society Paper No. 2266-61, October 9, 1961.
6. Jones, W. L., C. A. Aukerman, and J. W. Gibb, *Experimental Performance of a Hydrogen-Fluorine Rocket Engine at Several Chamber Pressures and Exhaust Nozzle Area Ratios,* NASA TM X-387, Washington, D. C., October, 1960 (CONFIDENTIAL).
7. *Nomad Semiannual Technical Program Report,* Report R-1388-3, Rocketdyne, Canoga Park, Calif., December 31, 1959 (CONFIDENTIAL).
8. Ponsford, H. T., R. M. Wood, R. E. Lowe, and J. F. Madewell, *Thermostructural Design—Entry Vehicles for Mars and Venus,* American Rocket Society Paper No. 1092-60, April, 1960.
9. Seifert, H. S., *Space Technology,* John Wiley and Sons, Inc., New York, 1959.
10. Wrobel, J. R., and R. R. Breshears, *Lunar Landing Vehicle Propulsion Requirements,* Technical Release No. 34-66, Jet Propulsion Laboratory, Pasadena, Calif., May 1, 1960.
11. Clarke, V. C., *Design of Lunar and Interplanetary Ascent Trajectories,* Technical Report No. 32-30, Jet Propulsion Laboratory, Pasadena, Calif., July 26, 1960.
12. Lorell, J., *Two–Dimensional Analysis of Interplanetary Flight Schedules,* Memorandum No. 30-13, Jet Propulsion Laboratory, Pasadena, Calif., December 1. 1959.